Double-Stream Differential Chaos Shift Keying Communications Exploiting Chaotic Shape Forming Filter and Sequence Mapping

Chao Bai, Xiao-Hui Zhao, Hai-Peng Ren, *Senior Member, IEEE*, Géza Kolumbán, *Fellow, IEEE*, and Celso Grebogi

Abstract

A new Differential Chaos Shift Keying modulation scheme exploiting Chaotic Shape-forming Filter and Sequence Mapping (CSF-SM-DCSK) is being proposed. The new CSF-SM-DCSK system employs a novel sequence mapping rule and includes a data correction module to achieve a good trade-off between the low Bit Error Rate (BER) performance and high transmission rate. It transmits two data streams simultaneously and preserves the simplicity and robustness of DCSK method. Channel one, transmitting a Low Priority Stream (LPS), generates the chaotic carrier by a Chaotic Shape-forming Filter (CSF) at the transmitter and applies a coherent Matched Filter (MF) at the receiver to recover the information. Channel two, transmitting a High Priority Stream (HPS), relies on conventional DCSK modulation, while the reference and information-bearing parts are transmitted simultaneously with orthogonal sine and cosine carriers. This double-stream solution eliminates the need for analog RF delay lines and doubles the data transmission rate. Before feeding the LPS data stream into the modulator, each LPS bit is encoded into a symbol sequence using sequence mapping. This approach, together with the coherent MF reception, equips the LPS channel with an extremely high robustness against channel noise and multipath propagation. To handle every possible redundancy in the received signal and to minimize the possibility of making wrong decisions, a data correction block is also introduced. Initially, a rough estimation of the received HPS DCSK bit is done at

C. Bai is with the Xi'an Key Laboratory of Intelligent Equipment, Xi'an Technological University, Xi'an 710021, China (e-mail: baic@xatu.edu.cn).

X. H. Zhao is with the Shaanxi Key Laboratory of Complex System Control and Intelligent Information, Xi'an University of Technology, Xi'an 710048, China (e-mail: qq362323557@163.com).

H. P. Ren is with the Xi'an Key Laboratory of Intelligent Equipment, Xi'an Technological University, Xi'an 710021, China, and also with the Shaanxi Key Laboratory of Complex System Control and Intelligent Information, Xi'an University of Technology, Xi'an 710048, China (e-mail: renhaipeng@xaut.edu.cn).

G. Kolumbán is with the Faculty of Information Technology and Bionics, Pázmány Péter Catholic University, Budapest, Hungary (e-mail: kolumban@itk.ppke.hu) and he is an Adjunct Prof. at the School of Engineering, Edith Cowan University, Perth, Australia.

C. Grebogi is with the Institute for Complex Systems and Mathematical Biology, University of Aberdeen AB24 3UE, United Kingdom (e-mail: grebogi@abdn.ac.uk).

Manuscript received July 19, 2020; revised August 26, 2020.

the receiver, then this estimation is used to remove the DCSK modulation from the received information-bearing signal. The three inputs of data correction blocks are: (i) the reference and (ii) the information-bearing parts of the received signal in their original form, and (iii) the received information-bearing signal where the DCSK modulation is removed. The data correction block improves the BER performance while the increased channel capacity, enabled by the double-stream approach, improves the spectral efficiency. Analytical expressions are derived to predict the BER performances in additive white Gaussian noise channel for both the LPS and HPS channels. Computer simulations are used to show that the system performance of the CSF-SM-DCSK modulation scheme proposed in this work is superior to that of the already published solutions. In addition to the computer simulations, the new chaos-based wireless communications system has been implemented on a wireless open-access research platform to experimentally demonstrate the feasibility and the superiority of CSF-SM-DCSK.

Index Terms

Chaotic shape-forming filter, matched filter, sequence mapping, DCSK, chaotic communications.

I. Introduction

CHAOTIC signals have been being used in communication systems for the last three decades since Pecora-Caroll proposed the first chaos-synchronization method [1] in 1990 and Hayes-Grebogi conceptualized the idea of communications with chaos [2] in 1993. The inherently wideband chaotic signals offer many unique features in spread spectrum communications such as low probability of detection [3], mitigation of multipath fading [4], [5] and resistance to jamming [6].

A large number of chaotic modulation schemes have been proposed in the past three decades [7]. The inherently wideband chaotic carriers have not only been successfully used in commercial optical fiber communications [8] but have also been applied in the latest international standard elaborated for Wireless Body Area Networks (WBANs) referred to as IEEE Std 802.15.6 [9]. Among the chaos-based communication schemes published until now, the non-coherent Differential Chaos Shift Keying (DCSK) method [10] is the most popular one and it offers the most robust chaos-based solution to spread spectrum communications [11]. The excellent robustness of DCSK originates from its operation principle, each bit to be transmitted is encoded into two chaotic waveforms, referred to as reference and information-bearing signals, and the information bit is encoded into the sign of the correlation measured between the two transmitted chaotic waveforms. The DCSK modulation can be used even in time-variant channels provided that the channel parameters do not change too much during the successive transmission of the two waveforms. However, DCSK has three serious drawbacks: (i) it is a non-coherent communications scheme where both the reference and information-bearing signals are corrupted by the channel noise [12],

(ii) the wideband delay lines required in both the transmitter and receiver are difficult to implement by the current Complementary Metal Oxide Semiconductor (CMOS) technology [13], and (iii) DCSK offers only a halved data rate since each bit is transmitted by two successive waveforms [14].

Noise Reduction DCSK (NR-DCSK) was proposed in [12] to enhance the Bit Error Rate (BER) performance of DCSK. Both the reference and information bearing signals are transmitted P-times and their averages are used in the demodulation. Averaging reduces the effect of noise and, consequently, improves the BER performance. However, NR-DCSK reduces the attainable data rate by a factor of the repeating times.

A lot of research efforts have been devoted to the elimination of delay lines in DCSK. The idea of Time Division Multiplexing (TDM) is used in DCSK to transmit the reference and information-bearing signals in an isolated manner. In addition to TDM, many other techniques have been proposed to implement two isolated transmission channels. In Improved DCSK (I-DCSK) [15], the time-reversal operation is used to generate two orthogonal chaotic waveforms, where one of them is used as the reference while the other one is the information-bearing signal. Because of their orthogonality, the reference and information-bearing signals can be transmitted in the same time slot. Therefore, delay lines are not required either in the transmitter or in the receiver. Another I-DCSK feature is that the simultaneous transmission of the two signals doubles the data rate. Unfortunately, I-DCSK is very sensitive to multipath propagation which prevents its use in mobile and indoor applications [16]. In Phase-Separated DCSK (PS-DCSK) [17], the two orthogonal channels are implemented by means of sine and cosine auxiliary carriers that are used to transmit the reference and information-bearing signals simultaneously in an isolated manner. However, the matched filter used in PS-DCSK demodulator can be optimized only for single-path propagation; therefore, the PS-DCSK performance degrades seriously in multipath propagation environments.

Other researchers have focused on increasing the data rate attainable by DCSK. Very High Efficiency-DCSK (VHE-DCSK) [18], High-data rate Code Shifted DCSK (HCS-DCSK) [19] and Generalized Correlation Delay Shift Keying (GCDSK) [20] modulations belong to this class of DCSK, where the delta function-like autocorrelation property of chaotic signals is exploited. Unfortunately, the BER performance of these systems deteriorates severely with the increasing number of orthogonal carriers and the implementations need many delay lines.

Frequency Division Multiplexing (FDM) has been used successfully in Multi-Carrier DCSK (MC-DCSK) [21], Carrier Index DCSK (CI-DCSK) [22], Sub-carrier Allocated MC-DCSK (SA-MC-DCSK) [23] and Repeated Spreading Sequence MC-DCSK (RSS-MC-DCSK) [24] to improve the Bit Transmission

Rate (BTR) at the expense of increased channel bandwidth.

Square-constellation-based M-ary DCSK (M-DCSK) [25] and Multi-level Code-Shifted DCSK (MCS-DCSK) [26] have also been proposed to increase the data rate by mapping multiple information bits into a certain constellation, i.e., symbol. The cost to be paid is the increasing system complexity and deteriorated BER performance.

Recent discoveries of some special properties of chaotic signals have opened up new application possibilities in wireless chaos-based communications. It has been shown that the information entropy of chaotic signals remains unaltered during its transmission over a radio channel. Therefore, chaotic signals can be used as carrier signals in radio communications [27]. Chaotic carriers can be generated by Chaotic Shape-forming Filters (CSFs), which enable the use of matched filter-based demodulators in order to get the best BER performance attainable theoretically in an AWGN channel [28], [29].

In multipath wireless communications, the CSF-based systems offer a better system performance than their conventional competitors while their complexity does not exceed that of the conventional radio transceivers [30]. The Lyapunov spectrum invariance property of chaotic signals in wireless channels can be exploited to mitigate the Inter-Symbol Interference (ISI) caused by multipath propagation [31]. A significant improvement in BER performance has been observed in both simulations and experiments when the CSF approach was used to replace the conventional communications technologies relying on square-root-raised-cosine pulse shaping transmit filters and applying the minimum mean square error-type channel equalization [30], [32]. ISI and BER performance can be enhanced further by using artificial intelligence and machine learning [33]–[35].

The CSF has been first applied to DCSK in [16], referred to as Second Order Hybrid System DCSK (SOHS-DCSK). Two data streams are transmitted simultaneously where one data stream is encoded into chaotic waveforms by the CSF and the other one is modulated by conventional DCSK. The SOHS-DCSK provides much higher BTR than the other enhanced DCSK systems. However, the BER of data stream transmitted by CSF is seriously deteriorated in multipath channels. To overcome the problem and implement a multi-level DCSK (CSF-M-DCSK) modulation scheme [36], a Walsh coding has been added. Compared to SOHS-DCSK, the CSF-M-DCSK improves significantly the BER performance and increases the channel capacity.

The CSF-SM-DCSK modulation scheme proposed here includes all ideas of chaos-based communications surveyed above and in order to further improve the system performance, three brand-new ideas are introduced:

(i) Two parallel data communication channels transmitting the low and high priority bit streams are implemented where the information data streams formed by sequence mapping are conveyed by both the reference and information-bearing signals of DCSK modulation;
(ii) Sequence Mapping (SM) is used to encode the bits of low priority stream into more than one symbols to improve the BER performance by redundancy, i.e., by averaging;
(iii) A new Data Correction (DC) block is added to the demodulator to exploit all redundancy available in the received signals in order to further improve the overall system performance.

CSF-SM-DCSK transmits two data stream simultaneously, the Low Priority and High Priority Streams denoted by LPS and HPS, respectively. Each LPS bit is mapped into a symbol sequence and the data transmission is performed in information frames, where each frame transmits several LPS bits and one HPS bit carried by DCSK modulation. The chaotic carrier is generated neither by logistic [37], [38] nor by tent [39]–[41] maps, instead, each symbol generated by SM is fed directly into a CSF to get the analog modulated chaotic LPS waveforms. The DCSK modulation transmits each HPS bit in such a way that the analog modulated chaotic LPS waveform is used as the chaotic carrier fed into the DCSK modulator.

The idea of hierarchical modulation was proposed and extensively investigated [42]. Hierarchical modulation assures different qualities of services for the parallel information bit streams depending on their levels of importance. System performance analysis of hierarchical modulation in Additive White Gaussian Noise (AWGN) channel was published in [43], where a rotation approach was used to outperform the BER of conventional communications systems [44].

In recent years, hierarchical modulation was combined with chaos-based modulation to get a multi-level DCSK (MR-M-DCSK) system [45]. The non-uniformly spaced constellation points and the different levels of priorities were assigned by setting different distances among the constellation points in that solution. An adaptive transmission scheme was proposed in [46], where the distances of neighboring constellation points were controlled. A search algorithm was proposed in [47] to select the optimum positions of constellation points depending on the signal-to-noise ratio.

The difference between the hierarchical modulation approach and the method proposed here are twofold:
(i) Conventional hierarchical modulation achieves unequal error protection by assigning different energy for the different layer. Because the total energy used to transmit one symbol is fixed, the transmission reliability is significantly affected by the energy allocated to a layer. If the BER in one layer is decreased, then the BERs in other layers are getting worse. However, the BERs measured in the HPS and LPS channels of the CSF-SM-DCSK have no influence on each other and a data correction module is used

at the receiver to enhance the BER performances in both streams; (ii) In the hierarchical modulations proposed up to now, similar modulation technique is used in each layer. However, CSF-SM-DCSK uses completely different modulation schemes in the HPS and LPS channels.

To eliminate the need for analog delay lines, not the TDM concept but two orthogonal carriers, i.e., sine and cosine functions, are used to transmit the reference and information-bearing parts of the DCSK signal. Because the two parts are transmitted simultaneously, they undergo the same distortion in the radio channel; consequently, their correlation is not corrupted by the channel distortion. Note, this approach does not extend the occupied frequency band but doubles the data rate in the HPS DCSK channel.

A unique feature of CSF-SM-DCSK modulation is that the analog modulated chaotic LPS waveform is used as carrier in the DCSK modulator. Due to the double-transmission of LPS waveform, a redundancy exists which is exploited in the receiver to improve the BER performance. The receiver first separates the reference and information-bearing parts of the received signal and demodulates both of them by a coherent matched filter. Then the HPS bit is estimated by a DCSK demodulator and the estimated HPS bit is used to recover an unmodulated version of the information-bearing signal. Hence, the demodulator provides three data streams: (i) the modulated LPS sequence, which is also used as the reference part of DCSK signal, (ii) the modulated LPS sequence, which is recovered from the information-bearing part of DCSK signal by removing the DCSK modulation, and (iii) the information-bearing part of DCSK signal. The three data streams are processed by the data correction block, which exploits all redundant information available in the received signals and makes the decision in favor of both LPS and HPS bits, assuring the minimum probability of making wrong decisions.

The paper is organized as follows: The operation principle of the new CSF-SM-DCSK system is discussed in Sec. II. The analytical equations giving the BER performances for both the LPS and HPS data streams are derived in Sec. III. Verification of the theoretical BER performances and their comparison with that of the already published chaos-based DCSK schemes are given in Sec. IV. Experimental validation of the feasibility of CSF-SM-DCSK and its performance evaluation in a real application scenario are done in Sec. V. Conclusions are drawn in Sec. VI.

II. CSF-SM-DCSK CONFIGURATION

A. The transmitter description

The block diagram of the proposed CSF-SM-DCSK transmitter is shown in Fig. 1. The incoming digital information is transmitted in frames where N LPS bits and one HPS bit form one information frame. Let

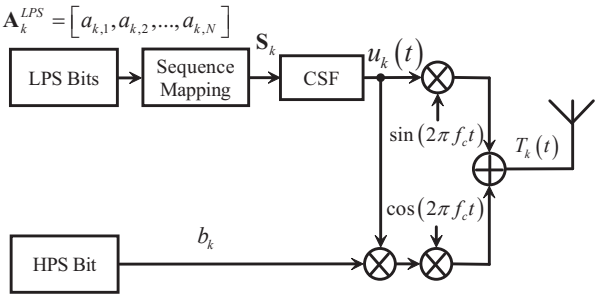

Fig. 1. Block diagram of the CSF-SM-DCSK transmitter showing the transmission of the kth information frame $\mathbf{S}_k$.

T_a and T_b denote the duration of one LPS and one HPS bits, respectively, where $T_b \geq T_a$. As shown in Fig. 1, $N = T_b/T_a$ LPS bits denoted by $\mathbf{A}_k^{LPS} = [a_{k,1}, a_{k,2}, \ldots, a_{k,N}]$ and one HPS bit marked by b_k are transmitted in the kth information frame. Note that both the transmission and the demodulation of one information frame are performed in one step. In general $N > 1$, but in the simplest case only one LPS bit is used to carry one HPS bit, i.e., $N = T_b/T_a = 1$.

Each LPS bit is mapped into a predefined symbol in the SM module to improve the robustness of CSF-SM-DCSK system against the channel imperfections. The SM module multiplies each incoming LPS bit by a predefined and fixed spreading code

$$\mathbf{\Phi} = [\phi_1, \phi_2, ..., \phi_P], \tag{1}$$

where P is the LPS sequence mapping or spreading gain, and the elements of spreading code are given by $\phi_p \in \{\pm 1\}$ $(1 \leq p \leq P)$. The generation method of spreading code is arbitrary, it can be derived from a chaotic or random sequence, or even from a deterministic one. The SM module can be implemented by a multiplier; its output is obtained as

$$\begin{aligned} \mathbf{S}_k &= [a_{k,1}\mathbf{\Phi}, a_{k,2}\mathbf{\Phi}, ..., a_{k,N}\mathbf{\Phi}] = [a_{k,1}(\phi_1, \phi_2, ..., \phi_P), \\ &a_{k,2}(\phi_1, \phi_2, ..., \phi_P), ..., a_{k,N}(\phi_1, \phi_2, ..., \phi_P)] \\ &= [s_{k,1}, s_{k,2}, ..., s_{k,m}, ..., s_{k,M}], \end{aligned} \tag{2}$$

where $s_{k,m} \in \{\pm 1\}$ is the mth bipolar symbol in $\mathbf{S}_k$, and M is the spreading gain in the HPS channel. Note, the spreading gains in the LPS and HPS channels differ from each other. The structure of the kth transmitted information frame is shown in Fig. 2. The kth information frame carries one HPS bit b_k and N LPS bits $[a_{k,1}, a_{k,2}, ..., a_{k,N}]$, where each LPS bit is mapped into a spreading code sequence $[\phi_1, \phi_2, ..., \phi_P]$. Consequently, $M = PN$ symbols are transmitted in the kth information frame $\mathbf{S}_k = [s_{k,1}, s_{k,2}, ..., s_{k,m}, ..., s_{k,M}]$.

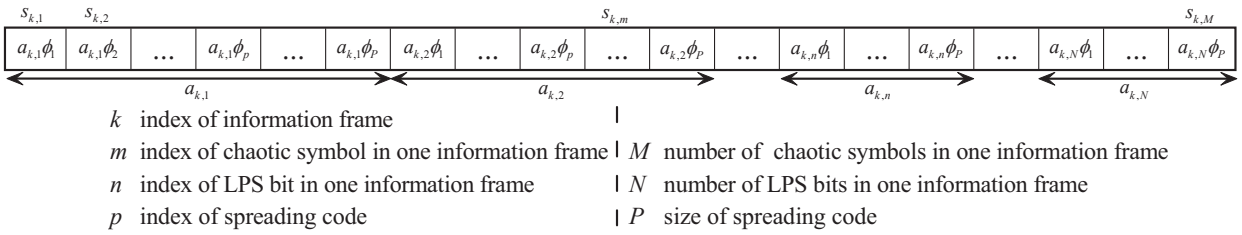

Fig. 2. Structure of the kth information frame.

In wireless communications, the modulator maps the symbol sequence to be transmitted into an analog waveform. Here a CSF [16], [30] is used as modulator, its input signal is equal to the reference part of the kth information frame. For the kth information frame, the CSF output carrying the LPS modulation is obtained as

$$u_k(t) = \sum_{m=\lfloor t \rfloor}^{\lfloor t \rfloor + \infty} s_{k,m+1} \delta(t-m), \tag{3}$$

where $u_k(t)$ is the output of the CSF for the kth information frame, $\lfloor t \rfloor$ indicates the largest integer less than or equal to t, and $\delta(t)$ is the basis function of CSF given by

$$\delta(t) = \begin{cases} \left(1-e^{-\frac{\beta}{f}}\right) e^{\beta t} \left(\cos(\omega t) - \frac{\beta}{\omega}\sin(\omega t)\right), & t < 0 \\ 1 - e^{\beta\left(t-\frac{1}{f}\right)} \left(\cos(\omega t) - \frac{\beta}{\omega}\sin(\omega t)\right), & 0 \le t < \frac{1}{f} \\ 0, & t \ge \frac{1}{f} \end{cases}. \tag{4}$$

In Eq. (4), f is the base frequency of the basis function, which determines the duration $1/f$ of one symbol, $\omega = 2\pi f$, and $\beta = f \cdot \ln 2$. Figure 3 shows the basis function by a blue solid curve. Note, its value is negligible when $t < -6$. The value of the basis function rapidly decays along the negative time axis. Let N_δ denote the magnitude of time rounded to the closest integer where $\delta(t)$ is negligible. Then, in Eq. (3), the upper limit of summation becomes $N_\delta = 6$ and the value of the basis function can be neglected beyond that limit. Note, the duration of one transmitted information frame carrying one HPS bit and N LPS bits is PN/f.

As shown in Figs. 1 and 2, the LPS bit stream spread by the spreading code $\mathbf{\Phi}$ and mapped into an analog waveform $u_k(t)$ by CSF is used as chaotic carrier in the DCSK modulator. The CSF output $u_k(t)$ gives the DCSK reference signal, while its product with the kth HPS bit b_k gives the information-bearing signal. The two parts of DCSK signal are transmitted simultaneously by using two orthogonal carriers, indicated by the sine and cosine functions in Fig. 1. The transmitted signal generated by the kth

This article has been accepted for publication in a future issue of this journal, but has not been fully edited. Content may change prior to final publication. Citation information: DOI 10.1109/TWC.2021.3135043, IEEE Transactions on Wireless Communications

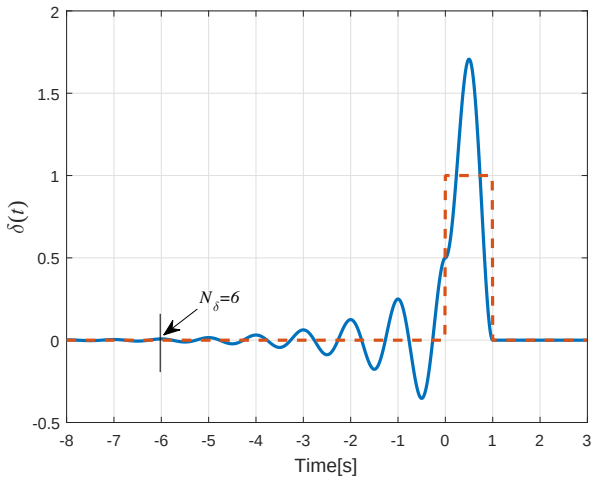

Fig. 3. Shape of the basis function with base frequency f=1 Hz. Note, if $t < -N_\delta = -6$, then $\delta(t)$ is negligible. The transmitted symbol is also shown by red dashed curve.

information frame is obtained as

$$T_k(t) = u_k(t)\sin(2\pi f_c t) + b_k u_k(t)\cos(2\pi f_c t), \quad (k-1)T_b \le t < kT_b, \tag{5}$$

where f_c is the frequency of the orthogonal sinusoidal carriers.

To illustrate the operation principle of CSF-SM-DCSK modulator with an example, let us consider the transmission of two information frames with the parameters shown in Table I, where two LPS and one HPS bits are used to form one information frame, i.e., $N = 2$. The two layers of modulation can be recognized in Fig. 1. The lower modulation layer transmits the LPS bit stream, where the LPS bits are spread by $\mathbf{\Phi}$ and the information frame $\mathbf{S}_k$ is converted into analog waveforms by the CSF. The upper modulation layer applies DCSK modulation to transmit the HPS bits, in such a way, the CSF output $u_k(t)$ is used by the DCSK modulator as carrier. The sequence mapping gain is determined by the size P of the spreading code which is equal to 2. Thus, $M = PN = 4$ symbols are transmitted in one information frame. The reference and information-bearing parts of DCSK carrying HPS bit are transmitted simultaneously with the sine and cosine auxiliary carriers, which form two orthogonal channels. Therefore, three information bits including one HPS bit and two LPS bits are transmitted in one information frame as shown in Table I.

The SM output can be determined from Eq. (2) or Fig. 2, its value for the two information frames considered here is $\mathbf{S}=[\mathbf{S}_1, \mathbf{S}_2] = [-1, 1, 1, -1, 1, -1, -1, 1]$. The HPS, LPS and $\mathbf{S}$ symbol sequences are shown in Fig. 4(a) by the blue solid, red dashed and cyan dotted curves, respectively.

The duration of one information symbol has been set to $T_b = 1s$ by the specification. Because $M =$

TABLE I
THE PARAMETERS OF THE ILLUSTRATION EXAMPLE.

Frame	LPS	HPS	T_a	T_b	$\mathbf{\Phi}$	N	P
1	$\mathbf{A}_1^{LPS} = [1, -1]$	$b_1 = 1$	0.5s	1s	[-1, 1]	2	2
2	$\mathbf{A}_2^{LPS} = [-1, 1]$	$b_2 = -1$					

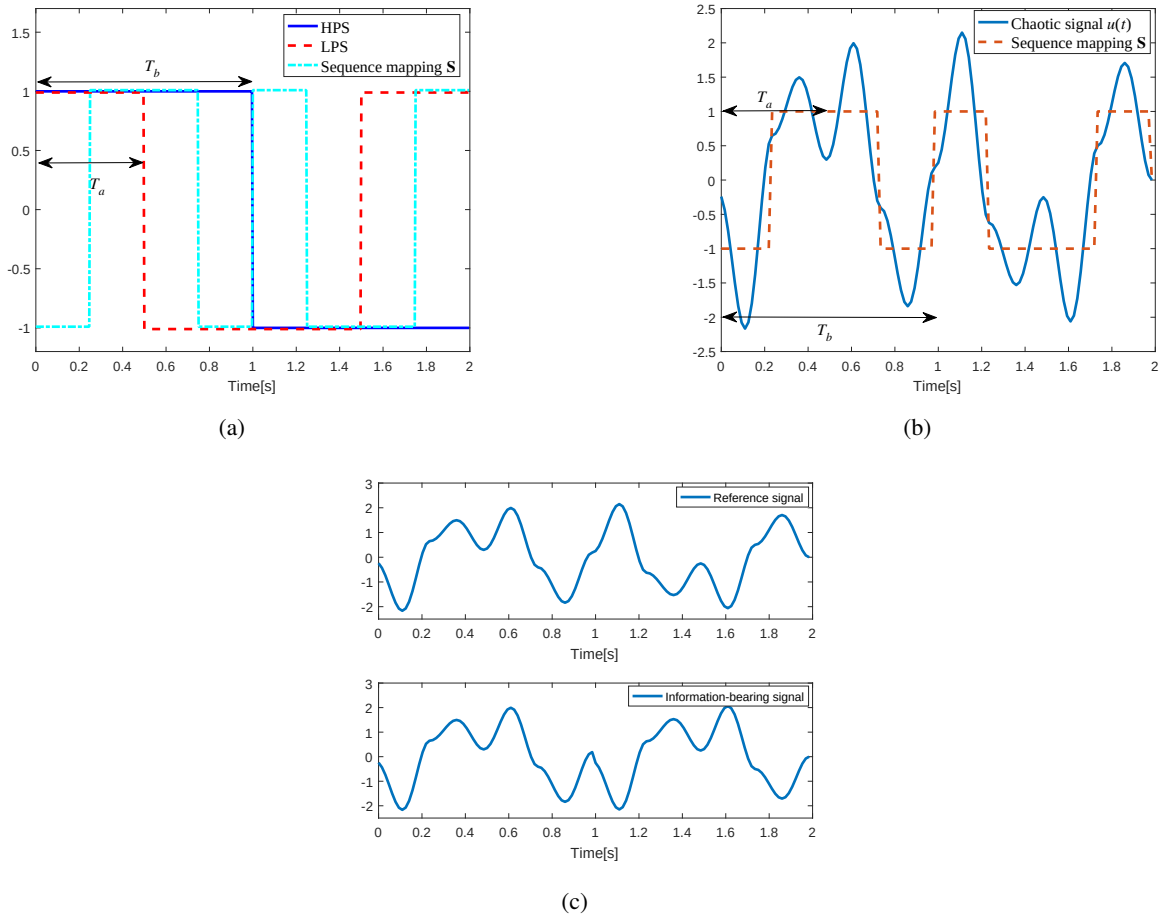

Fig. 4. Signals and waveforms in the CSF-SM-DCSK modulator: (a) the HPS, LPS and **S** symbol sequences are shown by the blue solid, red dashed and cyan dotted curves, respectively; (b) the **S** symbol sequence (red dashed curve) fed into CSF and its analog output $u(t)$ (blue solid curve); (c) the reference and information-bearing parts of transmitted DCSK signal. Note, the transmission of two information frames are shown in each figure and the DCSK reference signal is equal to the LPS modulated chaotic signal $u(t)$.

$NP = 4$ symbols are transmitted in one information frame, the base frequency f has to be set to 4Hz. As shown in Fig. 1, the output S of SM block is fed into CSF module which provides the LPS modulated chaotic signal $u(t)$, $0 \leq t < 2T_b$. Figure 4(b) depicts $u(t)$ together with **S** by blue solid and red dashed curves, respectively. Note, all waveforms plotted in Fig. 4 are generated by two information frames. The CSF-SM-DCSK modulation scheme uses the kth LPS modulated waveform $u_k(t)$ as DCSK carrier to transmit b_k. Therefore, the reference and information-bearing parts of DCSK signal corresponds to $u_k(t)$ and $b_k u_k(t)$, respectively. These components of DCSK signal are plotted in the upper and lower panels

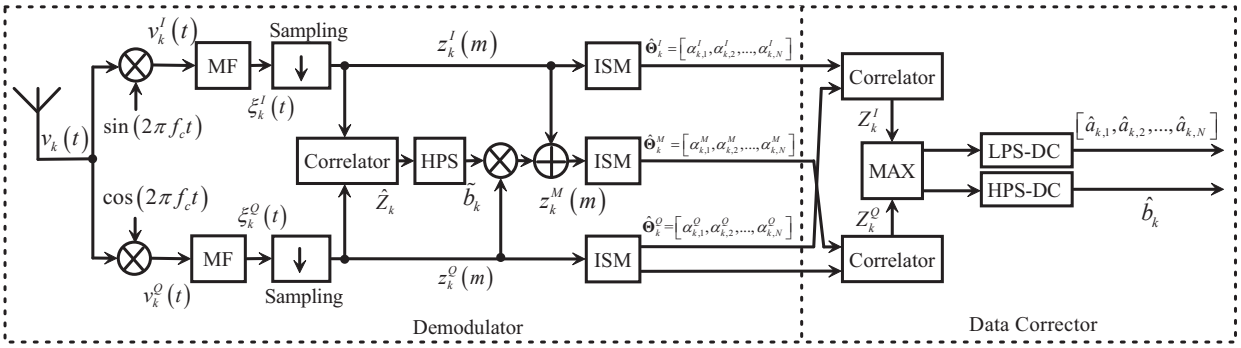

Fig. 5. Block diagram of the CSF-SM-DCSK receiver. Note, the input $z_k^M(m)$ of the middle ISM block is the sum of $z_k^I(m)$ and the remodulated $z_k^Q(m)$, where the HPS DCSK modulation $\hat{b}_k$ is removed from $z_k^Q(m)$ by the remodulation.

of Fig. 4(c), which are transmitted simultaneously with a sine and cosine orthogonal carrier as shown in Fig. 1.

B. The receiver description

The block diagram of the CSF-SM-DCSK receiver includes two parts: the demodulator and the data corrector units as shown in Fig. 5. The demodulator recovers three data sequences from the received noisy analog signal $v_k(t)$ captured by the antenna, and generates three parallel data sequences denoted by $\hat{\mathbf{\Theta}}_k^I$, $\hat{\mathbf{\Theta}}_k^M$, and $\hat{\mathbf{\Theta}}_k^Q$. These sequences carry all information which is available in the received signal $v_k(t)$, and they are processed by the data corrector unit to recover the transmitted HPS and LPS bits with a minimum probability of making wrong decisions.

Consider the reception of the kth information frame. The received signal $v_k(t)$, corrupted by channel noise and interferences, is down-converted by a quadrature mixer to separate and recover the reference and information-bearing parts of DCSK signals. These parts are processed in parallel, as shown in Fig. 5, where the upper and lower receiver arms are identified by the upper indices I and Q, respectively, in the remaining of the paper.

The upper and lower down-converter outputs denoted by $v_k^I(t)$ and $v_k^Q(t)$, respectively, are fed into two parallel Matched Filters (MFs) [48], [49]. Their outputs are obtained as

$$\xi_k^{(*)}(t) = \int_{-\infty}^{\infty} \delta(-\tau) v_k^{(*)}(t-\tau)\, d\tau, \tag{6}$$

where $(*)$ stands for I and Q, and the impulse response of both matched filters is the time-reverse of the basis function defined by Eq. (4). The MF outputs $\xi_k^I(t)$ and $\xi_k^Q(t)$ are sampled at the decision time

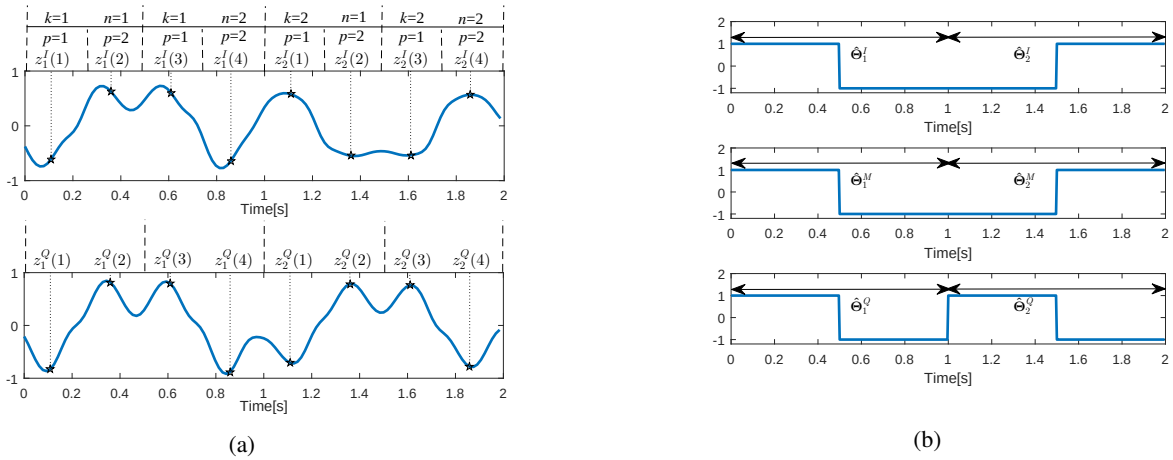

(a) (b)

Fig. 6. Waveforms and signals in the CSF-SM-DCSK receiver for two LPS bits, i.e., $N = 2$, are transmitted in one information frame and the size of spreading code $P = 2$. The figures illustrate the transmission of two information frames: (a) outputs of MF blocks are shown in the upper and lower panels by blue solid lines in the I and Q arms, respectively, the pentagon marks give the sampling points $z_k^I(m)$ and $z_k^Q(m)$ of I and Q sampling switches, respectively; (b) data sequences are recovered by the upper, middle and lower ISM blocks shown in upper, middle, and lower panels, respectively.

instants to get the decision vectors in both the reference and information bearing signals, respectively.

$$z_k^{(*)}(m) = \xi_k^{(*)}\left((k-1)T_b + \frac{m-1}{f} + \frac{1}{2f}\right), 1 \le m \le M. \tag{7}$$

Recall, because of the double-modulation approach, $z_k^I(m)$ and $z_k^Q(m)$ carry the LPS bits and, simultaneously, correspond to the received reference and information-bearing parts of DCSK signals. The analog MF outputs, $\xi_k^I(t)$ and $\xi_k^Q(t)$, together with the outputs of sampling switch $z_k^I(m)$ and $z_k^Q(m)$, are shown in Fig. 6(a) by blue solid curves and black pentagon marks, respectively. The upper and lower panels belong to $\xi_k^I(t)$ and $\xi_k^Q(t)$, respectively.

$z_k^I(m)$ and $z_k^Q(m)$ carry not only the LPS modulation but also the reference and information-bearing parts of HPS DCSK modulation. The correlation between $z_k^I(m)$ and $z_k^Q(m)$ returns the DCSK observation signal

$$\hat{Z}_k = \sum_{m=1}^{M} z_k^I(m)\, z_k^Q(m), \tag{8}$$

where $M = PN$ is the spreading gain in the HPS channel. The estimated HPS information $\tilde{b}_k$ is obtained as

$$\tilde{b}_k = \begin{cases} +1, & \hat{Z}_k \ge 0 \\ -1 & \hat{Z}_k < 0 \end{cases}. \tag{9}$$

The LPS data sequence has been spread by the sequence mapping code $\mathbf{\Phi}$ before transmission to improve

its robustness against a noisy multipath channel. Each spreading symbol of LPS data is transmitted two times using the orthogonal sine and cosine channels. The Inverse Sequence Mapping (ISM) modules recover the LPS data sequences with and without HPS DCSK modulation from the sampling points and HPS DCSK demodulator. To exploit all information available in the received signal, three LPS data sequence are recovered as shown in Fig. 5:

- $\hat{\mathbf{\Theta}}_k^I$ is derived by the upper ISM decoder directly from the reference signal sampling points, $z_k^I(m)$, it is an estimation of the transmitted $\mathbf{A}_k^{LPS}$ data sequence;
- $\hat{\mathbf{\Theta}}_k^M$ is derived from the sum of $z_k^I(m)$ and $\tilde{b}_k z_k^Q(m)$ through the middle ISM, where the HPS of DCSK modulation is removed by the estimating $\tilde{b}_k$ provided by Eq. (9), and the averaging always suppresses the effect of channel noise;
- $\hat{\mathbf{\Theta}}_k^Q$ is derived directly by the lower ISM decoder from $z_k^Q(m)$. Note, $\hat{\mathbf{\Theta}}_k^Q$ carries both the LPS and HPS DCSK modulations.

The three ISM blocks are identical coherent correlation decoders, which generate three parallel data sequences identified by the indices I, M and Q, respectively, in Fig. 5.

The predefined spreading code $\mathbf{\Phi}$ is *a priori* known at the CSF-SM-DCSK receiver. Figure 2 shows that N LPS bits are transmitted in one information frame where each LPS bit is multiplied by the spreading code. The three ISM blocks are coherent correlation decoders which correlate the three noisy LPS symbols carried by $z_k^I(m)$, $z_k^M(m)$ and $z_k^Q(m)$ with $\mathbf{\Phi}$, and generate three observation vectors. The elements of these observation vectors are given by

$$D_{k,n}^{(\cdot)} = \sum_{p=1}^{P} z_k^{(\cdot)}[P(n-1)+p]\phi(p),$$

where $(\cdot)$ stands for I, M and Q, i.e., for the upper, middle and lower ISM blocks, respectively. Each ISM block is equipped by a decision circuit which returns the estimates of received data sequences

$$\alpha_{k,n}^{(\cdot)} = \begin{cases} 1, & \text{if } D_{k,n}^{(\cdot)} \geq 0. \\ -1, & \text{if } D_{k,n}^{(\cdot)} < 0. \end{cases} \tag{10}$$

Note, $\hat{\mathbf{\Theta}}_k^I$ and $\hat{\mathbf{\Theta}}_k^M$ carry only the LPS bits but $\hat{\mathbf{\Theta}}_k^Q$ carries both the LPS and HPS DCSK modulations.

The BERs of LPS for the I and M arms shown in Fig. 5 are determined by the decision variables z_k^I and z_k^M, where the Probability Density Function (PDF) $f^I\left(z_k^I\right)$ and $f^M\left(z_k^M\right)$ for $E_b/N_0 = -5dB$ are given in Fig. 7 with blue solid line and red dashed line, respectively. In theory, the lower limit of BER is given by the minimum in $f^I\left(z_k^I\right)$ and $f^M\left(z_k^M\right)$ for the integration from $-\infty$ to 0, as given by the pink

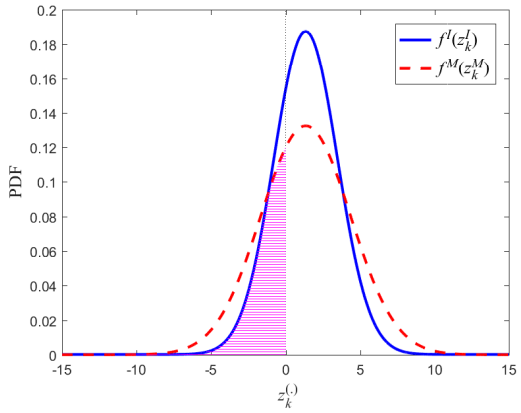

Fig. 7. The PDF of decision variable z_k^I and z_k^M under $E_b/N_0 = -5dB$.

area in Fig. 7. In practice, it cannot be guaranteed that the minimum of $f^I\left(z_k^I\right)$ and $f^M\left(z_k^M\right)$ is always selected. Therefore, in the DC module, the estimated data sequence $\hat{\mathbf{\Theta}}_k^Q$ is used as the reference vector, and $\hat{\mathbf{\Theta}}_k^I$ or $\hat{\mathbf{\Theta}}_k^M$ with higher correlation with $\hat{\mathbf{\Theta}}_k^Q$ is selected as the recovered DC information bits. The operation process is as follows:

From Eq. (10), the three estimated data sequences denoted by $\hat{\mathbf{\Theta}}_k^I = [\alpha_{k,1}^I, \alpha_{k,2}^I, ..., \alpha_{k,N}^I]$, $\hat{\mathbf{\Theta}}_k^M = [\alpha_{k,1}^M, \alpha_{k,2}^M, ..., \alpha_{k,N}^M]$ and $\hat{\mathbf{\Theta}}_k^Q = [\alpha_{k,1}^Q, \alpha_{k,2}^Q, ..., \alpha_{k,N}^Q]$ are obtained at the demodulator output. The three data sequences $\hat{\mathbf{\Theta}}_k^I$, $\hat{\mathbf{\Theta}}_k^M$ and $\hat{\mathbf{\Theta}}_k^Q$ are fed into the data correction unit, as shown in Fig. 5. Note, vectors $\hat{\mathbf{\Theta}}_k^I$ and $\hat{\mathbf{\Theta}}_k^M$ carry two different estimations of the same LPS bit sequence while $\hat{\mathbf{\Theta}}_k^Q$ carries both the LPS and HPS DCSK modulations.

The HPS DCSK bit is carried by the correlation measured between the reference and information-bearing parts of received signals. Because two estimations of the reference sequence are available, two values of correlations can be determined

$$\begin{cases} Z_k^I = \hat{\mathbf{\Theta}}_k^I (\hat{\mathbf{\Theta}}_k^Q)^{Tr} \\ Z_k^Q = \hat{\mathbf{\Theta}}_k^M (\hat{\mathbf{\Theta}}_k^Q)^{Tr} \end{cases}, \tag{11}$$

where the superscript Tr denotes the transpose operation. These correlation values are used in the DC unit to recover the transmitted HPS and LPS, i.e., to perform the decision.

The HPS bit is recovered by the DCSK detection algorithm

$$\hat{b}_k = \begin{cases} \operatorname{sgn}\left(Z_k^I\right), & \text{if } \left|Z_k^I\right| \geq \left|Z_k^Q\right| \\ \operatorname{sgn}\left(Z_k^Q\right), & \text{if } \left|Z_k^I\right| < \left|Z_k^Q\right| \end{cases}, \tag{12}$$

where sgn is the modified signum function

$$\mathrm{sgn}(Z) = \begin{cases} 1, & \text{if } Z \geq 0 \\ -1, & \text{if } Z < 0 \end{cases} . \tag{13}$$

Theoretically, both $\hat{\mathbf{\Theta}}_k^I$ and $\hat{\mathbf{\Theta}}_k^M$ carries the LPS bit sequences. This redundancy is exploited by applying the following decision in the recovery of LPS bits

$$\hat{a}_{k,n} = \begin{cases} \alpha_{k,n}^I, & \text{if } \left|Z_k^I\right| \geq \left|Z_k^Q\right| \\ \alpha_{k,n}^M, & \text{if } \left|Z_k^I\right| < \left|Z_k^Q\right| \end{cases} . \tag{14}$$

The operation principle of CSF-SM-DCSK modulator is illustrated by the transmission of two information frames in Table I. The analog waveforms and data sequences generated by these frames in the demodulator are depicted in Fig. 6 for the noise-free case. The reference and information-bearing parts of the information frames transmitted via the sine and cosine channels, respectively, are assigned by the sampling switches placed after the matched filter and are denoted by pentagon marks in Fig. 6(a). These estimations, denoted by $z_k^I(m)$ and $z_k^Q(m)$, are de-spread by the *a priori* known $\mathbf{\Phi}$ to get the estimations of $\hat{\mathbf{\Theta}}^I = \left[\hat{\mathbf{\Theta}}_1^I, \hat{\mathbf{\Theta}}_2^I\right] = [1, -1, -1, 1]$ and $\hat{\mathbf{\Theta}}^Q = \left[\hat{\mathbf{\Theta}}_1^Q, \hat{\mathbf{\Theta}}_2^Q\right] = [1, -1, 1, -1]$, which are shown in the upper and lower panels of Fig. 6(b). The middle panel in Fig. 6(b) shows $\hat{\mathbf{\Theta}}^M = [1, -1, -1, 1]$ recovered from the received signal transmitted via the orthogonal sine and cosine channels and where the HPS DCSK modulation has been removed. Then these estimation, $\hat{\mathbf{\Theta}}^I$, $\hat{\mathbf{\Theta}}^Q$ and $\hat{\mathbf{\Theta}}^M$ are used by the decision algorithms defined by Eqs. (11)-(14) to recover the LPS and HPS bits.

III. BER ANALYSIS OF THE CSF-SM-DCSK SYSTEM

In the bit error rate performance analysis, we assume that a single isolated CSF-SM-DCSK information frame is transmitted. The BER evaluation is performed in three steps: BER analysis of (i) the HPS channel, (ii) the LPS channel, and (iii) the effect of data correction.

A. BER analysis of the HPS channel

The sine and cosine carriers shown in Fig. 1, have two roles: (i) they establish the two orthogonal channels required by the simultaneous transmission of the two parts of DCSK signal, and (ii) they assign the center frequency f_c of transmitted signal. The quadrature down-converter in the receiver shown in Fig. 5 recovers the two parts of CSF-SM-DCSK waveforms. In the BER analysis, the noise contribution of the receiver is merged into the channel noise.

The transmitted signal passes through a wireless multipath Rayleigh fading channel characterized by its impulse response

$$h\left(t\right)=\sum_{l=1}^{L}\lambda_{l}\psi\left(t-\tau_{l}\right), \tag{15}$$

where L is the number of parallel propagation paths. The radio channel considered here has slow fading where the lth path is characterized by its channel fading coefficient λ_l and time delay τ_l, and $\psi\left(\cdot\right)$ is the Dirac delta function. The Rayleigh probability density function of channel coefficient is given by

$$f_{\lambda}\left(z\right)=\frac{z}{\sigma_{\lambda}^{2}}e^{-\frac{z^{2}}{2\sigma_{\lambda}^{2}}},$$

where $\sigma_\lambda > 0$ is the scale parameter of the distribution [50]. This radio channel model is commonly used to test the multipath performance of telecommunications systems [51]–[53].

In a multipath channel, the outputs of two down-converters generated by the kth information frame are

$$\begin{aligned}v_{k}^{I}\left(t\right)=&h\left(t\right)\otimes u_{k}\left(t\right)+w^{I}\left(t\right)=\sum_{l=1}^{L}\lambda_{l}u_{k}\left(t-\tau_{l}\right)+w^{I}\left(t\right)\\=&\sum_{l=1}^{L}\lambda_{l}\sum_{n=1}^{M}s_{k,n}\delta\left(t-\tau_{l}-n/f\right)+w^{I}\left(t\right)\end{aligned} \tag{16}$$

and

$$\begin{aligned}v_{k}^{Q}\left(t\right)=&h\left(t\right)\otimes b_{k}u_{k}\left(t\right)+w^{Q}\left(t\right)=\sum_{l=1}^{L}\lambda_{l}b_{k}u_{k}\left(t-\tau_{l}\right)+w^{Q}\left(t\right)\\=&\sum_{l=1}^{L}\lambda_{l}\sum_{n=1}^{M}b_{k}s_{k,n}\delta\left(t-\tau_{l}-n/f\right)+w^{Q}\left(t\right),\end{aligned} \tag{17}$$

where "$\otimes$" denotes the convolution operation, $w^I\left(t\right)$ and $w^Q\left(t\right)$ represent the additive white Gaussian noises which corrupt the reference and information-bearing signals, respectively. MF outputs generated by the kth information frame are obtained as

$$\begin{aligned}\xi_{k}^{I}\left(t\right)=&\int_{-\infty}^{\infty}\delta\left(-\tau\right)v_{k}^{I}\left(t-\tau\right)d\tau\\=&\sum_{l=1}^{L}\lambda_{l}\sum_{n=1}^{M}s_{k,n}\int_{-\infty}^{\infty}\delta\left(\tau\right)\delta\left(\tau-t+\tau_{l}+\tfrac{n}{f}\right)d\tau+\int_{-\infty}^{\infty}w^{I}\left(\tau\right)\delta\left(\tau-t\right)d\tau\end{aligned}$$

and

$$\begin{aligned}\xi_{k}^{Q}\left(t\right)=&\int_{-\infty}^{\infty}\delta\left(-\tau\right)v_{k}^{Q}\left(t-\tau\right)d\tau\\=&b_{k}\sum_{l=1}^{L}\lambda_{l}\sum_{n=1}^{M}s_{k,n}\int_{-\infty}^{\infty}\delta\left(\tau\right)\delta\left(\tau-t+\tau_{l}+\tfrac{n}{f}\right)d\tau+\int_{-\infty}^{\infty}w^{Q}\left(\tau\right)\delta\left(\tau-t\right)d\tau,\end{aligned}$$

where $\delta(t)$ is the basis function defined in Eq. (4) and $s_{k,n}$ is the nth bipolar symbol in the kth information frame. The decision vectors $\mathbf{z}_k^I$ and $\mathbf{z}_k^Q$ are obtained by sampling $\xi_k^I(t)$ and $\xi_k^Q(t)$, respectively, with the

sampling rate of $1/f$. The mth elements of the I and Q decision vectors in the kth frame

$$\begin{aligned} z_k^I(m) &= \sum_{l=1}^{L}\sum_{n=1}^{M} s_{k,n}C_{l,n-m} + W^I = \sum_{l=1}^{L} s_{k,m}C_{l,0} + \sum_{l=1}^{L}\sum_{\substack{n=1\\ n\neq m}}^{M} s_{k,n}C_{l,n-m} + W^I \\ &= s_{k,m}\Delta + \Xi_{k,m}^I + W^I \end{aligned} \tag{18}$$

and

$$\begin{aligned} z_k^Q(m) &= b_k\sum_{l=1}^{L}\sum_{n=1}^{M} s_{k,n}C_{l,n-m} + W^Q = b_k\sum_{l=1}^{L} s_{k,m}C_{l,0} + \sum_{l=1}^{L}\sum_{\substack{n=1\\ n\neq m}}^{M} b_k s_{k,n}C_{l,n-m} + W^Q \\ &= b_k s_{k,m}\Delta + \Xi_{k,m}^Q + W^Q, \end{aligned} \tag{19}$$

respectively, where $m = 1, 2, ...M$, M is the spreading gain in the HPS channel and

$$C_{l,n-m} = \lambda_l \int_{-\infty}^{\infty} \delta(\tau)\,\delta\left(\tau + \tau_l + \tfrac{n-m}{f}\right)d\tau = \begin{cases} \lambda_l D\left(2 - e^{-\frac{\beta}{f}} - e^{\frac{\beta}{f}}\right)\left(A\cos(\omega\tau_l) + B\sin(\omega\tau_l)\right), & \left|\tau_l + \frac{n-m}{f}\right| \geq \frac{1}{f} \\ \lambda_l \begin{bmatrix} A\left(D\left(2 - e^{-\frac{\beta}{f}}\right) - D^{-1}e^{-\frac{\beta}{f}}\right)\cos(\omega\tau_l) + \\ B\left(D\left(2 - e^{-\frac{\beta}{f}}\right) + D^{-1}e^{-\frac{\beta}{f}}\right)\sin(\omega\tau_l) + \\ 1 - |\tau_l f| + n - m \end{bmatrix}, & 0 \leq \left|\tau_l + \frac{n-m}{f}\right| < \frac{1}{f} \end{cases}. \tag{20}$$

In Eq. (20), $A = \frac{(\omega^2 - 3\beta^2)f}{4\beta(\omega^2+\beta^2)}$, $B = \frac{(3\omega^2 - \beta^2)f}{4\omega(\omega^2+\beta^2)}$ and $D = e^{-\beta\left|\tau_l + \frac{n-m}{f}\right|}$.

In the first terms of Eqs. (18) and (19), $\Delta = \sum_{l=1}^{L} C_{l,0} = \sum_{l=1}^{L} \lambda_l E$ is the sum of the multipath power for the mth symbol $s_{k,m}$, E is the signal energy of one symbol which is obtained from the autocorrelation function of basis function. The second terms $\Xi_{k,m}^I$ and $\Xi_{k,m}^Q$ are the Inter-Symbol Interferences (ISIs) appearing in the reference and the information-bearing signals, respectively. In a multipath channel, their values are obtained as

$$\begin{aligned} \Xi_{k,m}^I &= \sum_{l=1}^{L}\sum_{\substack{n=1\\ n\neq m}}^{M} s_{k,n}C_{l,n-m} = \underbrace{\sum_{l=1}^{L}\sum_{n=1}^{m-1} s_{k,n}C_{l,n-m}}_{I_{past}} + \underbrace{\sum_{l=1}^{L}\sum_{n=m+1}^{M} s_{k,n}C_{l,n-m}}_{I_{future}} \\ \Xi_{k,m}^Q &= b_k\sum_{l=1}^{L}\sum_{\substack{n=1\\ n\neq m}}^{M} s_{k,n}C_{l,n-m} = b_k\underbrace{\sum_{l=1}^{L}\sum_{n=1}^{m-1} s_{k,n}C_{l,n-m}}_{I_{past}} + b_k\underbrace{\sum_{l=1}^{L}\sum_{n=m+1}^{M} s_{k,n}C_{l,n-m}}_{I_{future}} \end{aligned}, \tag{21}$$

where I_{past} and I_{future} are the ISI from the past and future symbols, respectively. As shown in [16] and [31], they have uniform distribution given by

$$I_{past} \sim U\left(-\left|\frac{K}{e^{\frac{\beta}{f}} - 1}\right|, \left|\frac{K}{e^{\frac{\beta}{f}} - 1}\right|\right) \quad \text{and} \quad I_{future} \sim U\left(-\left|\frac{K}{e^{\frac{\beta}{f}} - 1}\right|, \left|\frac{K}{e^{\frac{\beta}{f}} - 1}\right|\right), \tag{22}$$

where

$$K=\sum_{l=1}^{L}\lambda_l\left(2-e^{-\frac{\beta}{f}}-e^{\frac{\beta}{f}}\right)e^{-\beta\tau_l}\left(A\cos\left(\omega\tau_l\right)+B\sin\left(\omega\tau_l\right)\right). \tag{23}$$

The last terms $W^{(*)}=\int_{-\infty}^{\infty}w^{(*)}\left(\tau\right)\delta\left(\tau-t\right)d\tau$ in Eqs. (18) and (19) are the filtered channel noises with zero mean and variance $\frac{N_0}{2}E$ [31], [54].

The HPS decision variable $\hat{Z}_k$ in the kth information frame is obtained as

$$\begin{aligned}\hat{Z}_k&=\sum_{m=1}^{M}\mathbf{z}_k^I\left(m\right)\mathbf{z}_k^Q\left(m\right)\\&=\sum_{m=1}^{M}\left(s_{k,m}\Delta+\Xi_{k,m}^I+W^I\right)\left(b_k s_{k,m}\Delta+\Xi_{k,m}^Q+W^Q\right)\\&=\sum_{m=1}^{M}\left(b_k s_{k,m}^2\Delta^2+s_{k,m}\Delta H^Q+b_k s_{k,m}\Delta H^I+H^I H^Q\right),\end{aligned} \tag{24}$$

where $H^{(*)}=\Xi_{k,m}^{(*)}+W^{(*)}$.

The expectation of Eq. (24) is

$$\begin{aligned}&E_{xp}\left(\hat{Z}_k\right)=ME_{xp}\left(b_k s_{k,m}^2\Delta^2\right)+ME_{xp}\left(s_{k,m}\Delta H^Q\right)\\&+ME_{xp}\left(b_k s_{k,m}\Delta H^I\right)+ME_{xp}\left(H^I H^Q\right),\end{aligned} \tag{25}$$

where $E_{xp}\left(\cdot\right)$ denotes the expectation operator. The expectations of the second, third, and fourth terms are zero in Eq. (25), because $E_{xp}\left(W^I\right)=E_{xp}\left(W^Q\right)=0$. Therefore, the expectation of the HPS decision variable is obtained as

$$E_{xp}\left(\hat{Z}_k\right)=M\Delta^2=M\sum_{l=1}^{L}\lambda_l^2E^2. \tag{26}$$

The signal energy in the kth information frame is $E_b^{HPS}=2ME$. Its substitution into Eq. (26) yields

$$E_{xp}\left(\hat{Z}_k\right)=\frac{1}{4M}\sum_{l=1}^{L}\lambda_l^2\left(E_b^{HPS}\right)^2. \tag{27}$$

The variance of $\hat{Z}_k$ is

$$\begin{aligned}&V_{ar}\left(\hat{Z}_k\right)\\&=MV_{ar}\left(b_k s_{k,m}^2\Delta^2\right)+MV_{ar}\left(s_{k,m}\Delta H^Q\right)+MV_{ar}\left(b_k s_{k,m}\Delta H^I\right)+MV_{ar}\left(H^I H^Q\right)\\&=M\Delta^2\left(F+\tfrac{N_0}{2}E\right)+M\Delta^2\left(F+\tfrac{N_0}{2}E\right)+M\left(F+\tfrac{N_0}{2}E\right)^2\\&=2MF\Delta^2+M\Delta^2N_0E+MF^2+\tfrac{1}{4}ME^2N_0^2+MFN_0E\\&=\tfrac{F}{2M}\sum_{l=1}^{L}\lambda_l^2\left(E_b^{HPS}\right)^2+\tfrac{N_0}{8M^2}\sum_{l=1}^{L}\lambda_l^2\left(E_b^{HPS}\right)^3+MF^2+\tfrac{\left(E_b^{HPS}\right)^2N_0^2}{16M}+\tfrac{1}{2}FE_b^{HPS}N_0,\end{aligned} \tag{28}$$

where $V_{ar}(\cdot)$ represents the variance operator and F gives ISI arising from the multipath propagation

$$F = V_{ar}\left(\Xi_{k,m}^{(*)}\right) = \begin{cases} 0, & \text{in AWGN channel} \\ \frac{2}{3}\left(\frac{K}{e^{\beta}-1}\right)^2, & \text{in multipath channel} \end{cases}. \tag{29}$$

The HPS bit error probability without data correction is obtained as

$$\begin{aligned} P_{HPS} &= \tfrac{1}{2}\mathrm{erfc}\left(\frac{E_{xp}\left(\hat{Z}_k\right)}{\sqrt{2V_{ar}\left(\hat{Z}_k\right)}}\right) \\ &= \tfrac{1}{2}\mathrm{erfc}\left(\frac{16MF}{\sum_{l=1}^{L}\lambda_l^2\left(E_b^{HPS}\right)^2} + 4\frac{N_0}{\sum_{l=1}^{L}\lambda_l^2 E_b^{HPS}} + \frac{32M^3F^2}{\sum_{l=1}^{L}\lambda_l^4\left(E_b^{HPS}\right)^4} + \frac{2MN_0^2}{\left(\sum_{l=1}^{L}\lambda_l^2 E_b^{HPS}\right)^2} + \frac{16M^2FN_0}{\sum_{l=1}^{L}\lambda_l^4\left(E_b^{HPS}\right)^3}\right)^{-\frac{1}{2}}, \end{aligned} \tag{30}$$

where $\mathrm{erfc}(\cdot)$ is the complementary error function, defined by

$$\mathrm{erfc}(x) = \frac{2}{\sqrt{\pi}}\int_x^{\infty} e^{-t^2}dt.$$

Finally, the BER performance of HPS channel implemented without DC is expressed in multipath radio channel as

$$\begin{aligned} &P_{HPS} \\ &= \int_0^{+\infty} \tfrac{1}{2}\mathrm{erfc}\left(\frac{16MF}{\gamma_b\left(E_b^{HPS}\right)^2} + 4\frac{N_0}{\gamma_b E_b^{HPS}} + \frac{32M^3F^2}{\gamma_b^2\left(E_b^{HPS}\right)^4} + \frac{2MN_0^2}{\left(\gamma_b E_b^{HPS}\right)^2} + \frac{16M^2FN_0}{\gamma_b^2\left(E_b^{HPS}\right)^3}\right)^{-\frac{1}{2}} f(\gamma_b)\, d\gamma_b, \end{aligned} \tag{31}$$

where $\gamma_b = \sum_{l=1}^{L}\lambda_l^2$ and $f(\gamma_b)$ is the PDF of γ_b. Because λ_l is a Rayleigh distributed random variable, $f(\gamma_b)$ can be obtained as done in [51].

The BER performance of the CSF-SM-DCSK HPS in an AWGN channel can be calculated from Eq. (30) by substituting L = 1, $\lambda = 1$ and F = 0

$$P_{HPS}^{AWGN} = \frac{1}{2}\mathrm{erfc}\left(4\frac{N_0}{E_b^{HPS}} + 2M\frac{N_0^2}{\left(E_b^{HPS}\right)^2}\right)^{-\frac{1}{2}}. \tag{32}$$

B. BER analysis of the LPS channel

Each LPS bit is transmitted two times via the I and Q channels. Therefore, the energy transmitted in one channel is $E^I = E^Q = \frac{E_b^{HPS}}{2M}P$. As shown in Fig. 5, each LPS bit is demodulated by a coherent matched filter receiver. Therefore, the PDF $f^I(x)$ and $f^Q(x)$ of $\mathbf{z}_k^I$ and $\mathbf{z}_k^Q$, respectively, follows Gaussian distribution with the expectation $E^I = E^Q$ and variances $\sigma^I = \sigma^Q = \sqrt{\frac{\Delta^2}{2}\frac{N_0}{E^I}} = \sqrt{\frac{M\Delta^2}{P}\frac{N_0}{E_b^{HPS}}}$ [16], [55]. The bit error

probabilities are identical in the I and Q channels

$$P^I = P^Q = \begin{cases} \frac{1}{4(E-1)^2}\left\{\begin{array}{c}\left[(2E-1)^2+\sigma^2\right]\operatorname{erfc}\left(\frac{(2E-1)}{\sigma\sqrt{2}}\right)\\ -2\left(E^2+\sigma^2\right)\operatorname{erfc}\left(\frac{E}{\sigma\sqrt{2}}\right)\\ +\left(1+\sigma^2\right)\operatorname{erfc}\left(\frac{1}{\sigma\sqrt{2}}\right)\end{array}\right\} & \text{in AWGN channel} \\ -\frac{\sigma}{4(E-1)^2}\sqrt{\frac{2}{\pi}}\left\{\begin{array}{c}(2E-1)\exp\left(-\frac{(2E-1)^2}{2\sigma^2}\right)\\ -2E\exp\left(-\frac{E^2}{2\sigma^2}\right)+\exp\left(-\frac{1}{2\sigma^2}\right)\end{array}\right\}, & \\ \sqrt{2\sigma^2}\frac{e^{\frac{\beta}{f}}-1}{4|K|}\left\{z_1\cdot erfc\left(z_1\right)-z_2\cdot erfc\left(z_2\right)-e^{-z_1^2}/\sqrt{\pi}+e^{-z_2^2}/\sqrt{\pi}\right\}, & \text{in multipath channel} \end{cases} \tag{33}$$

where $\sigma=\sigma^I=\sigma^Q$, $E=1+\left(1-e^{-\beta}\right)\frac{\omega^2-3\beta^2}{2\beta(\omega^2+\beta^2)}$ [49], $z_1=\frac{\Delta+\frac{|K|}{e^{\beta/f}-1}}{\sqrt{2\sigma^2}}$ and $z_2=\frac{\Delta-\frac{|K|}{e^{\beta/f}-1}}{\sqrt{2\sigma^2}}$ [31].

The middle arm of Fig. 5 removes the HPS DCSK modulation and sums up the received signals in the I and Q channels; consequently, the energy carrying one LPS bit is $E^M=\frac{E_b^{HPS}}{M}P$. If a bit error occurs in HPS DCSK demodulation, then the BER of $\hat{\mathbf{\Theta}}_k^M$ is about 0.5. Taking into account the BER in HPS DCSK demodulation, the bit error probability in $\hat{\mathbf{\Theta}}_k^M$ detection is obtained as

$$\begin{aligned} P^M=&\tfrac{1}{2}\Pr\left(\tilde{b}_k,error\right)+\tfrac{1}{2}\Pr\left(\alpha=1|a=-1\right)\Pr\left(\tilde{b}_k,right\right)\\ &+\tfrac{1}{2}\Pr\left(\alpha=-1|a=+1\right)\Pr\left(\tilde{b}_k,right\right)\\ =&\tfrac{1}{2}\int_{-\infty}^{0}f_{b_k}\left(x\right)dx+\left(1-\int_{-\infty}^{0}f_{b_k}\left(x\right)dx\right)\int_{-\infty}^{0}f\left(x\right)dx, \end{aligned} \tag{34}$$

where $f_{b_k}\left(x\right)$ is the PDF of HPS DCSK decision variable $\hat{Z}_k$ defined by Eq. (24). Its expectation and variance are given by Eq. (27) and Eq. (28), respectively. The PDF of $\hat{\mathbf{\Theta}}_k^M$, denoted by $f\left(x\right)$, has a Gaussian distribution with a variance of $\sigma=\sigma^M=\sqrt{\frac{\Delta^2}{2}\frac{N_0}{E^M}}=\sqrt{\frac{M\Delta^2}{2P}\frac{N_0}{E_b^{HPS}}}$ [36].

Then, the bit error probability of $\hat{\mathbf{\Theta}}_k^M$ can be rewritten as

$$P^M=\frac{1}{2}P_{HPS}+\left(1-P_{HPS}\right)P_e, \tag{35}$$

where P_{HPS} is given by Eq. (31) and P_e is obtained by substituting $P_e=P^I$ in Eq. (33) with a variance of $\sigma=\sigma^M$. The PDF of Eq. (34) can be approximated by $f^M\left(x\right)=\frac{1}{2}f_{b_k}\left(x\right)+f\left(x\right)$.

C. BER analysis of the data correction

The DC block exploits the redundancy buried in $\hat{\mathbf{\Theta}}_k^I$, $\hat{\mathbf{\Theta}}_k^Q$ and $\hat{\mathbf{\Theta}}_k^M$ to improve the BER in both the HPS and LPS channels. The correct LPS bits are recovered directly from the $\hat{\mathbf{\Theta}}_k^I$ and $\hat{\mathbf{\Theta}}_k^M$ data streams, while the data correction in the HPS channel depends on $\hat{\mathbf{\Theta}}_k^I$, $\hat{\mathbf{\Theta}}_k^Q$ and $\hat{\mathbf{\Theta}}_k^M$, as shown by Eqs. (12) and

(14). Therefore, the bit error probability measured in the LPS channel has to be evaluated first.

Let P_{LPS-DC} and P_{HPS-DC} denote the bit error probabilities measured after data correction in the LPS and HPS channels, respectively. When $N=1$ then $Z_k^I{=}Z_k^Q$ or $Z_k^I{=}-Z_k^Q$ and $\left|Z_k^I\right| = \left|Z_k^Q\right| = 1$ because $\hat{\mathbf{\Theta}}_k^I{=}\pm 1$ and $\hat{\mathbf{\Theta}}_k^M{=}\pm 1$, respectively. Consequently, the LPS bit error probability is equal to P^I according to Eq. (14).

If $N>1$, then the DC block improves the BER performance and the bit error probability in the LPS channel is obtained as

$$\begin{aligned} P_{LPS-DC} &= \Pr\left(\tilde{b}_k, rigth\right) P_{rig}^{LPS} + \Pr\left(\tilde{b}_k, error\right) P_{err}^{LPS} \\ &= \left(1-P_{HPS}\right) P_{rig}^{LPS} + P_{HPS} P_{err}^{LPS}, \end{aligned} \tag{36}$$

where P_{rig}^{LPS} and P_{err}^{LPS} are the bit error probabilities of LPS-DC when the estimated bit $\tilde{b}_k$ is right and wrong, respectively. Assume that the estimation of $\tilde{b}_k$ is perfect. Then the decision rule Eq. (14) is applied to get the best LPS BER performance. Equation (14) shows that the LPS-DC bit error probability is determined by either the I or M arms depending on the magnitudes of Z_k^I and Z_k^Q.

When the estimation of $\tilde{b}_k$ is false, then the probabilities of selecting $\alpha_{k,n}^I$ and $\alpha_{k,n}^M$ in Eq. (14) are given by

$$G_1 = \frac{\frac{N^2}{2}+2N+1}{\left(N+1\right)^2} \tag{37}$$

and

$$G_2 = \frac{N^2}{2\left(N+1\right)^2}, \tag{38}$$

respectively. The lower bound of the bit error probability for LPS-DC is given by

$$\begin{aligned} P_{LPS-DC}^{\text{Limit}} &= \left(1-P_{HPS}\right) \int_{-\infty}^{0} \min\left(f^I\left(x\right), f^M\left(x\right)\right) dx \\ &\quad + P_{HPS}\left(G_1 P^I + G_2 P^M\right). \end{aligned} \tag{39}$$

In summary, the bit error probabilities in the LPS channel after data correction are obtained as

$$\begin{aligned} P_{LPS-DC} &= P^I, && \text{if} \quad N=1 \\ P_{LPS-DC}^{\text{Limit}} &= \left(1-P_{HPS}\right) \int_{-\infty}^{0} \min\left(f^I\left(x\right), f^M\left(x\right)\right) dx \\ &\quad + P_{HPS}\left(G_1 P^I + G_2 P^M\right), && \text{if} \quad N>1 \end{aligned} \tag{40}$$

Next, the bit error probability of HPS demodulator, including data correction, is calculated. The bit error probability of HPS-DC demodulation is determined by the decision rule given in Eq. (12). For $N=1$, a false decision is made if the decision of either $\hat{\mathbf{\Theta}}_k^I$ or $\hat{\mathbf{\Theta}}_k^Q$ is false, therefore, the bit error probability is

obtained as

$$\begin{aligned} P_{HPS-DC} &= \Pr\left(\hat{\mathbf{\Theta}}_k^I, error\right)\Pr\left(\hat{\mathbf{\Theta}}_k^Q, right\right) + \\ &\Pr\left(\hat{\mathbf{\Theta}}_k^I, right\right)\Pr\left(\hat{\mathbf{\Theta}}_k^Q, error\right) \\ &= P^I\left(1-P^Q\right) + \left(1-P^I\right)P^Q. \end{aligned} \tag{41}$$

If $N > 1$, then the bit error probability is given by

$$P_{HPS-DC} = \Pr\left(\tilde{b}_k, rigth\right)P_{rig}^{HPS} + \Pr\left(\tilde{b}_k, error\right)P_{err}^{HPS}, \tag{42}$$

where P_{rig}^{HPS} and P_{err}^{HPS} are the HPS-DC bit error probabilities when the estimation of $\tilde{b}_k$ is perfect and false, respectively. The first term is much smaller than the second one under high SNR and can be ignored. When $\tilde{b}_k$ error occurs, $P_{err}^{HPS} = (G_1 P_{Z^I} + G_2 P_{Z^Q})$, where P_{Z^I} and P_{Z^Q} are the bit error probabilities of $\mathrm{sgn}\left(Z_k^I\right)$ and $\mathrm{sgn}\left(Z_k^Q\right)$ defined in Eq. (12), respectively, and G_1 and G_2 are given in Eqs. (37) and (38), respectively. The bit error probabilities P_{Z^I} and P_{Z^Q} are given by

$$\begin{aligned} P_{Z^I} \approx &\sum_{i=0}^{N}\sum_{j=0}^{N}\tfrac{N!}{i!(N-i)!}\left(P^I\right)^i\left(1-P^I\right)^{N-i}\tfrac{N!}{j!(N-j)!}\left(P^Q\right)^j\left(1-P^Q\right)^{N-j} \\ &-\left(1-P^I\right)^N\left(1-P^Q\right)^N - \left(P^I\right)^N\left(P^Q\right)^N \end{aligned} \tag{43}$$

and

$$\begin{aligned} P_{Z^Q} \approx &\sum_{i=0}^{N}\sum_{j=0}^{N}\tfrac{N!}{i!(N-i)!}\left(P^M\right)^i\left(1-P^M\right)^{N-i}\tfrac{N!}{j!(N-j)!}\left(P^Q\right)^j\left(1-P^Q\right)^{N-j} \\ &-\left(1-P^M\right)^N\left(1-P^Q\right)^N - \left(P^M\right)^N\left(P^Q\right)^N \end{aligned}. \tag{44}$$

From Eqs. (43) and (44), the lower bound of HPS-DC bit error probability is obtained as

$$P_{HPS-DC}^{\text{Limit}} = (1-P_{HPS})\,(G_1 P_{Z^I} + G_2 P_{Z^Q}). \tag{45}$$

In summary, the bit error probabilities in the HPS channel after data correction are obtained as

$$\begin{cases} P_{HPS-DC} = P^I\left(1-P^Q\right) + \left(1-P^I\right)P^Q, & N=1 \\ P_{HPS-DC}^{\text{Limit}} = (1-P_{HPS})\left(G_1 P_{Z^I} + G_2 P_{Z^Q}\right), & N>1 \end{cases}. \tag{46}$$

IV. Verification and Performance Comparison by Computer Simulations

A. BER performance evaluation and comparison in AWGN channel

AWGN channel and computer simulations are used in this section to verify the theoretical BER performances of CSF-SM-DCSK modulations in both the LPS and HPS channels, and to compare its system performance with its peers known from the literature. The parameters of the CSF-SM-DCSK considered here are given in Table II. The sampling frequency used in the computer simulations is set

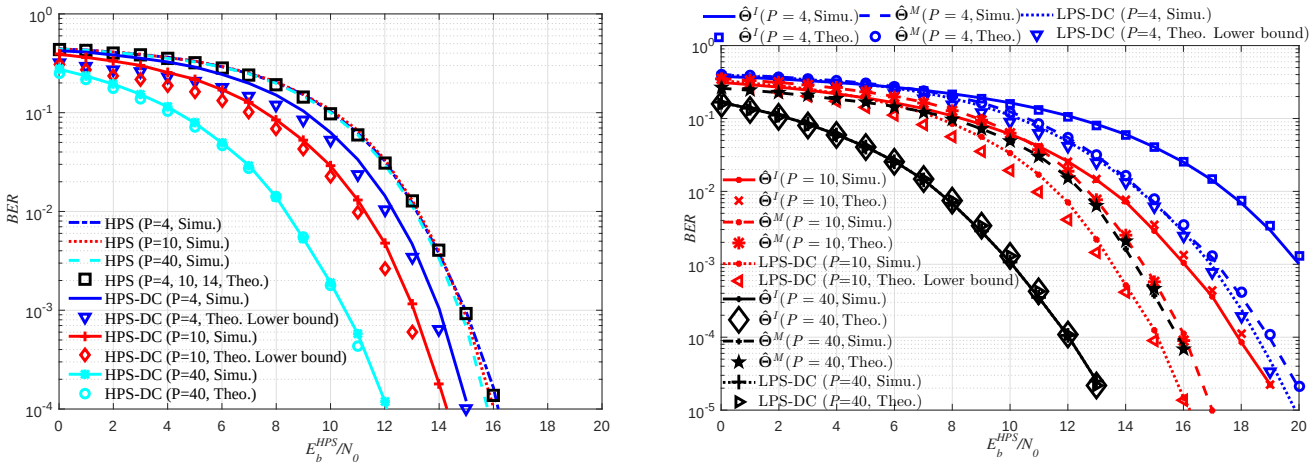

(a) (b)

Fig. 8. The BER performances of CSF-SM-DCSK modulation scheme in an AWGN channel. The BER performance of systems (a) HPS/HPS-DC and (b) LPS/LPS-DC. The length of information frame is M = 40 and the parameter P is the length of the spreading code.

TABLE II
PARAMETERS OF CSF-SM-DCSK SYSTEMS CONSIDERED IN COMPUTER SIMULATIONS.

Spreading gain	Bit Transmission Rate (bits/s)		f_c	f	f_s
M= 40, P = 4	625000 (LPS)	62500 (HPS)	5 MHz	2.5 MHz	40 MHz
M = 40, P = 10	250000 (LPS)	62500 (HPS)	5 MHz	2.5 MHz	40 MHz
M = 40, P = 40	62500 (LPS)	62500 (HPS)	5 MHz	2.5 MHz	40 MHz

at 40 MHz. Three chaotic spreading codes generated by Logistic map are used in simulations, where the lengths P of spreading codes are set to 4, 10 and 40. The BER performances in the HPS/HPS-DC and LPS/LPS-DC channels are plotted against the energy per one HPS bit to noise power spectral density ratio (E_b^{HPS}/N_0) measured in the HPS channel in Figs. 8(a) and 8(b), respectively, where $E_b^{HPS} = 2ME$. Both of them are in a very good agreement with the theoretical predictions given by Eqs. (31) and (46) for the HPS/HPS-DC, and Eqs. (33), (35) and (40) for the LPS/LPS-DC demodulators. Figure 8(a) shows that if data correction is not used, the BER performance in HPS channel does not depend on the size P of spreading code. However, if the data correction block is switched on, then the BER performance is improved by increasing P.

Figure 8(b) depicts the BER curves of the two data sequences $\hat{\Theta}_k^I$, $\hat{\Theta}_k^M$ and that in the LPS-DC channel. When the data correction block is not used then $\hat{\Theta}_k^I$ or $\hat{\Theta}_k^M$ is used to perform the demodulation in the LPS channel. The BER curves show that the application of data correction always improves the BER performance. The length of information frame M has been set to 40 in the simulations. If P = M = 40, then only one LPS bit is transmitted in one frame and the DC block cannot improve the BER performance. This fact is well reflected in Fig. 8(b) where the BER performance of $\hat{\Theta}_k^I$ and the LPS-DC are identical.

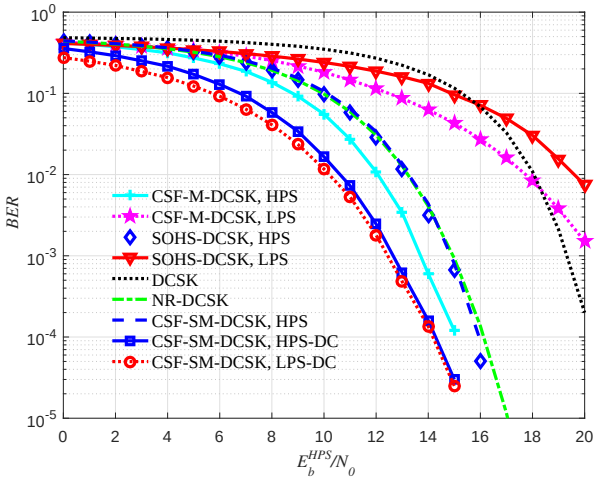

Fig. 9. Comparison of the BER performance of CSF-SM-DCSK modulation proposed in this work with that of its peers.

The Bit Transmission Rate (BTR) measured in the LPS/LPS-DC and HPS/HPS-DC channels are also identical in this case, but the BER performance of the LPS-DC channel outperforms that of the HPS-DC one. For large $N = M/P$, the BER performance of $\hat{\mathbf{\Theta}}_k^M$ outperforms that of $\hat{\mathbf{\Theta}}_k^I$ and tends toward the BER performance of the LPS-DC channel, as shown in Fig. 8(b) for P = 4. However, this performance gain is lost gradually when P is increased.

Figure 9 compares the BER performances of the proposed CSF-SM-DCSK, conventional DCSK [10], NR-DCSK [12], SOHS-DCSK [16] and CSF-M-DCSK [36] modulations in AWGN channel. The system parameters used in the performance comparison are given in Table III. Note, CSF-SM-DCSK, CSF-M-DCSK and SOHS-DCSK offer both HPS and LPS channels while DCSK and NR-DCSK implements only one channel. Figure 9 shows that the AWGN BER performances of the compared modulation schemes can be classified into three groups. The original version of DCSK, SOHS-DCSK LPS and CSF-M-DCSK LPS modulations offer the worst BER performances. Recall, the DCSK demodulator is a simple correlator and coding is not used to improve its robustness against channel noise. CSF-SM-DCSK HPS, CSF-M-DCSK HPS, SOHS-DCSK HPS and NR-DCSK belong to the second group which offers an improved BER performance compared to the first one. The physical explanation is obvious: CSF-SM-DCSK HPS, CSF-M-DCSK HPS and SOHS-DCSK HPS use coherent matched filter receiver while averaging is applied in NR-DCSK to improve the noise performance. Note, the BER of the CSF-M-DCSK HPS shows slightly better performance than CSF-SM-DCSK HPS, SOHS-DCSK HPS and NR-DCSK due to the use of maximum likelihood decision rule. The best BER performance is achieved by the third group which includes CSF-SM-DCSK modulation and employs data correction. The superior noise performance is achieved by DC, therefore, both LPS and HPS channels belong to this group. The improvement in E_b^{HPS}/N_0 varies from 1 to

TABLE III
PARAMETERS OF DIFFERENT DCSK MODULATIONS CONSIDERED FOR PERFORMANCE COMPARISON.

Method	BTR (bits/s)		Spreading gain	f_c	f	f_s
	LPS	HPS				
CSF-SM-DCSK	125000	62500	640(M= 40, P = 20)	5 MHz	2.5 MHz	40 MHz
NR-DCSK	-	31250	640 (P = 20)	-	-	40 MHz
DCSK	-	31250	640	-	-	40 MHz
SOHS-DCSK	2500000	62500	640 (M= 40)	5 MHz	2.5 MHz	40 MHz
CSF-M-DCSK	1250000	62500	640 (D = 2)	5 MHz	2.5 MHz	40 MHz

3 dB in the BER region which is used in mobile communications. Beyond the superior BER performance, the CSF-SM-DCSK modulation proposed here offers further advantages: (i) it implements an additional LPS-DC channel, and (ii) in contrast to CSF-M-DCSK and SOHS-DCSK LPS, its BER performance is improved by data correction in both the HPS and LPS channels.

B. BER performance evaluation in a multipath radio channel

This paragraph compares the BER performance of CSF-SM-DCSK, CSF-M-DCSK, conventional DCSK, NR-DCSK and SOHS-DCSK modulation schemes in a multipath radio channel. The parameters of DCSK systems considered here are given in Table III. The multipath radio channel used in the simulations has three propagation paths with average power gains [0.6, 0.3, 0.1] and excess delays [0μs, 0.1μs, 0.225μs], respectively [27].

Figure 10 shows that the BER performances predicted by the closed-form theoretical equations are in a good agreement with the simulated ones for high SNR. However, the prediction error increases when the SNR is deteriorated. This observation is valid for both the HPS-DC and LPS-DC channels. The phenomenon follows from the operation principle of the DC unti. If SNR is low, then the probability that DC uses a false reference vector increases.

Figure 10 shows that the multipath performances of CSF-M-DCSK HPS, NR-DCSK and SOHS-DCSK HPS modulations schemes are much better than that of the CSF-M-DCSK LPS, conventional DCSK and SOHS-DCSK LPS ones. The new CSF-SM-DCSK outperforms even the CSF-M-DCSK HPS, NR-DCSK and SOHS-DCSK HPS modulations schemes in multipath environments in both the HPS and LPS channels. The new CSF-SM-DCSK modulation scheme offer a 1-3dB gain in multipath performance. This performance improvement is mostly provided by the data correction block.

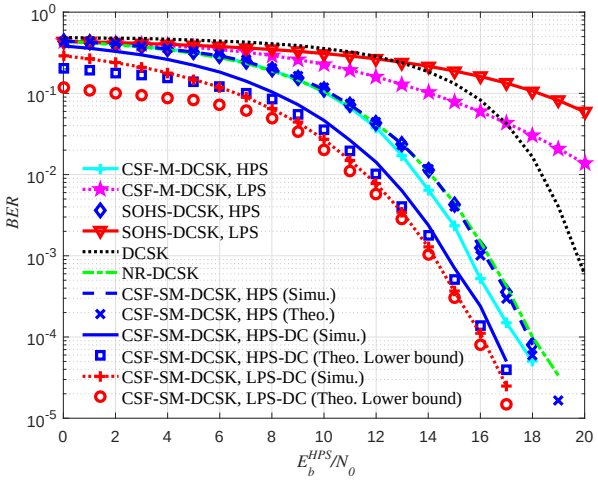

Fig. 10. BER performance comparison in a multipath radio channel.

C. Effect of spreading gain on BER, data rate and bit energy

The effect of LPS spreading gain P on BER, data rate and bit energy are simulated and analyzed in this subsection. One information frame transmits 1 HPS and N LPS bits simultaneously. The signal energy of one information frame is $E_b^{HPS} = 2ME$, where $E = \int_{-\infty}^{\infty} \delta(-\tau)\,\delta(t-\tau)d\tau = 1 + \left(1 - e^{-\beta}\right) \frac{\omega^2 - 3\beta^2}{2\beta(\omega^2+\beta^2)}$. The energy-per-bit is given by $E_{bit} = \frac{E_b^{HPS}}{N+1} = \frac{2ME}{N+1} = \frac{2MEP}{M+P}$, and is shown by black dashed line identified with pentagrams in Fig. 11.

The simulation results of the BER and BTR versus P variation under the same channel configuration as in Sec. IV-B are shown in Fig. 11, where the spreading gain M in the HPS channel has been set to 40. We see that, when spreading gain P is small, the performance of LPS-DC is worse than HPS-DC, but with a higher bit transmission rate. The bit transmission rate of LPS decreases gradually with the increasing of P, and the BER decreases rapidly due to the sequence mapping, while the bit transmission rate of HPS is identical without being affected by P. In general, the larger the P, the lower the BER in the LPS channel. Theoretically, when $P = M/2$, the BER of the LPS should be similar to that of the HPS, because the LPS is transmitted both in the reference signal and in the information bearing signal, which are transmitted in two separated carriers and used together in DC operation. But thanks to the DC operation, the transmission reliability of both HPS and LPS are improved. Therefore, the LPS-DC achieves better BER performance before P reaches $M/2$, as shown in Fig. 11.

D. Computational complexity comparison

The computational complexity of the proposed CSF-SM-DCSK is analyzed and compared with the DCSK, NR-DCSK, SOHS-DCSK and CSF-M-DCSK. The complexity $O(\cdot)$ of a method (algorithm) can

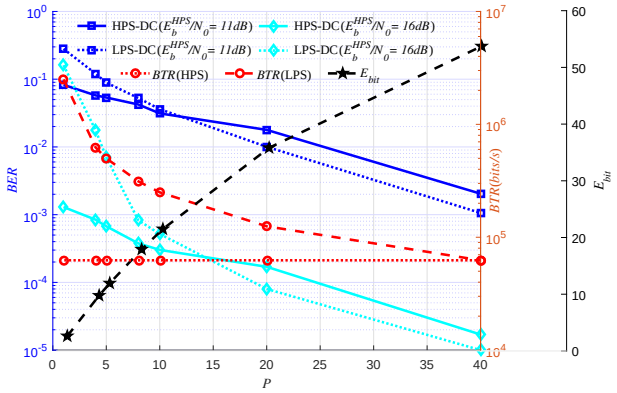

Fig. 11. The energy-per-bit and BER performance as a function of the length P of spreading code.

be defined as the number of multiplication and summation required to perform to detect one information bit. We assume here that N_β sampling points are used at the receiver to detect one information frame.

Many DCSK-based systems have been published up to now, their system complexities are compared in this section. To make the comparison tractable, one paragraph will be devoted to each DCSK modulation scheme to summarize its characteristics and the system parameter which determines the complexity of the given receiver will be shown as the argument of complexity parameter $O(\cdot)$.

In traditional DCSK, one bit is transmitted in one frame and the demodulation is performed by a correlator. The receiver complexity depends on the number of sampling points: $O\left(N_\beta\right)$.

In NR-DCSK, N_β sampling points are divided into ρ groups with a mean filter, and the receiver complexity is obtained as $O\left(N_\beta\right)+O\left(\rho\right)$.

In SOHS-DCSK, M+1 information bits are transmitted in one frame. The receiver is divided into two parts: i) the matched filters and ii) the decoding module. The complexity of two MFs used in the receiver is $O\left(\frac{2N_sN_\delta N_\beta}{(1+M)}\right)$. An M-point correlation operation is performed in demodulation, the overall receiver complexity is $O\left(\frac{M}{(1+M)}\right)$.

In PS-DCSK, one bit is transmitted in each frame and the structure of the receiver is similar to that of SOHS-DCSK. The complexity of MFs and the decoding process are $O\left(2N_sN_\delta N_\beta\right)$ and $O\left(M\right)$, respectively.

In CSF-M-DCSK, $\log_2 D + M/D$ bits are transmitted in one frame, where D is the dimension of the walsh code used in spreading. Then the complexity of MF is $O\left(\frac{N_sN_\delta N_\beta}{(\log_2 D+M/D)}\right)$, the decoding is performed by correlation, the receiver complexity is $O\left(\frac{2DM}{(\log_2 D+M/D)}\right)$.

In CSF-SM-DCSK proposed here, 1+M/P information bits are transmitted in one frame. The complexity of the two MFs is $O\left(\frac{2N_sN_\delta N_\beta}{(1+M/P)}\right)$. The receiver includes a demodulator block and a data corrector

TABLE IV
COMPUTATIONAL COMPLEXITY OF COMPARISON SCHEMES.

Method	Matched filter (MF)	Decoding
DCSK	no	$\mathrm{O}\left(N_\beta\right)$
NR-DCSK	no	$\mathrm{O}\left(N_\beta\right)+\mathrm{O}\left(\rho\right)$
PS-DCSK	$\mathrm{O}\left(2N_sN_\delta N_\beta\right)$	$\mathrm{O}\left(M\right)$
SOHS-DCSK	$\mathrm{O}\left(\frac{2N_cN_\delta N_\beta}{(1+M)}\right)$	$\mathrm{O}\left(\frac{M}{(1+M)}\right)$
CSF-M-DCSK	$\mathrm{O}\left(\frac{N_cN_\delta N_\beta}{(\log_2 D+M/D)}\right)$	$\mathrm{O}\left(\frac{2DM}{(\log_2 D+M/D)}\right)$
CSF-SM-DCSK	$\mathrm{O}\left(\frac{2N_cN_\delta N_\beta}{(1+M/P)}\right)$	$\mathrm{O}\left(\frac{4M}{(1+M/P)}\right)$

unit. The total complexity of the receiver is $O\left(\frac{4M}{(1+M/P)}\right)$.

The complexities of enhanced DCSK systems considered above are compared in Table IV. If the different systems are sorted by their complexity, then we get the following order: DCSK $<$ NR-DCSK $<$ CSF-MDCSK $<$ SOHS-DCSK $<$ CSF-SM-DCSK where DCSK has the simplest computational complexity.

The main source of computational complexity is the implementation of matched filters. If the MF is implemented by analog circuits [48], [49], then the complexity of CSF-SM-DCSK becomes significantly lower. For parameters which are used in real applications the order of receiver complexities is: SOHS-DCSK $<$ CSF-SM-DCSK $<$ CSF-M-DCSK $<$ DCSK $<$ NR-DCSK where SOHS-DCSK has the simplest computing complexity. CSF-SM-DCSK with analog MF has a moderate complexity, but in return, the moderate complexity of CSF-SM-DCSK gives outstanding BER and BTR performances.

E. Effect of the type of LPS spreading code on BER

The effect of the type of LPS spreading code on the CSF-SM-DCSK multipath performance is determined by computer simulation in this subsection. Three LPS spreading codes are considered: (i) a periodic sequence where $\phi_p = (-1)^p, p = 1, 2, ..., P$, (ii) the Gold sequence, and (iii) quantized sequence of a chaotic signal generated by Logistic map. The length of each spreading code has been set to P = 20. The other CSF-SM-DCSK system parameters are given in Table III and the characteristics of three-ray multipath channel considered in these simulations are identical with those ones discussed in the previous subsection. The multipath performances achieved by the three codes are compared in Fig. 12. Because of its discrete spectrum, the periodic LPS spreading code gives a very pure multipath performance. The pseudo random codes gives a much better multipath performance. Therefore, always a Gold code or a chaotic sequence has to be used in multipath propagation environments. Note, the multipath performances of the two pseudo random codes are almost identical.

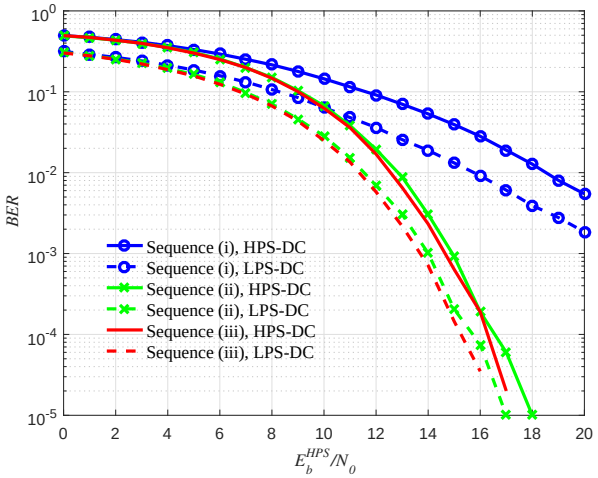

Fig. 12. Effect of the type of LPS spreading code on the multipath performance in the CSF-SM-DCSK modulation scheme. The BER performance are shown for (i) periodic sequence, (ii) Gold code, and (iii) chaotic sequence derived from a Logisitc map.

V. Experimental result measured on a Wireless Open-Access Research Platform

In order to validate the feasibility of the new CSF-SM-DCSK modulation scheme proposed in this work, a complete radio link has been implemented on a Wireless Open-Access Research Platform (WARP) [56]. The WARP testbed has also been used to evaluate the system performance of CSF-SM-DCSK in a real application environment and to compare it with that of its peers known from the literature. The photo of one WARP device is shown in Fig. 13(a). Each WARP includes a Xilinx Virtex-6 LX240T FPGA for signal processing, two MAX2829 RF chips to implement a 2.4 GHz/5 GHz dual-band transceiver, and DACs operating with a sampling rate of 40 MHz. The block diagram of the experimental setup is depicted in Fig. 13(b). The CSF-SM-DCSK, DCSK, NR-DCSK and SOHS-DCSK modulators and demodulators are implemented on the computer, which is connected to the two WARP units via the Ethernet switch. Note, a complete real radio link is implemented where the antenna connected to WARP1 radiates the modulated RF signal and, after passing the radio channel, it is picked up by the antenna of WARP2 which operates as a receiver. To ensure a fair comparison in the continuously varying radio channel, a test frame including all modulated signals is generated. As shown in Fig. 14, the modulated CSF-SM-DCSK, DCSK, NR-DCSK and SOHS-DCSK signals considered in this experiments transmit 50 bits each in one test frame and the 50 bits long information frames are separated by synchronization sequences. The synchronization sequences generated by a Logistic map are used to perform the frame synchronization and to cancel the frequency offset existing between the transmitter and receiver. The parameters of modulation schemes compared in the field tests are given in Table V. The photo of the experimental scenario is shown in Fig. 15(a), where the locations of two WARP devices are marked by red ellipsoids, and the computer used to

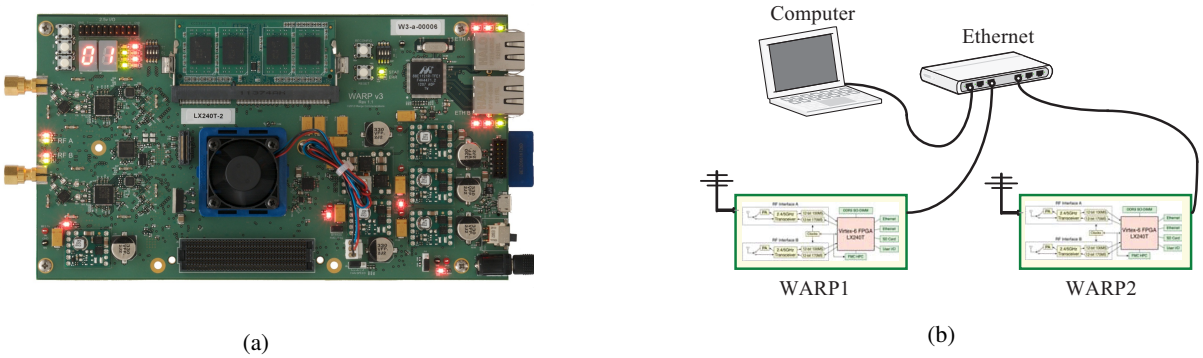

Fig. 13. Experimental validation of the feasibility of CSF-SM-DCSK system proposed in this work. (a) The photo of the WARP and (b) the block diagram of the experimental setup.

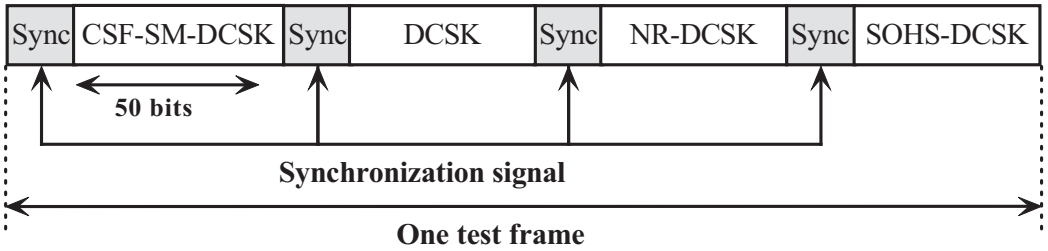

Fig. 14. Structure of test frame used in the field test.

generate the modulated test frames and demodulate the received signals is identified by a blue ellipsoid.

The results of field tests are shown in Fig. 15(b) for the conventional DCSK, NR-DCSK, SOHS-DCSK and CSF-SM-DCSK modulation schemes. The parameters of the real physical radio channel could not be varied in the experiment, therefore, the transmitted power has been changed to get the BER curves. The worst BER performance has been achieved in the LPS channel of the SOHS-DCSK modulation scheme, while the conventional DCSK has offered a quite good BER performance. As expected from simulations, NR-DCSK and the HPS channel of SOHS-DCSK outperforms the BER performance of DCSK by about 1dB. The best system performances have been achieved by CSF-SM-DCSK in both the LPS and HPS channels provided that the data correction block is used after the demodulator. The results of field tests

TABLE V
THE PARAMETERS CONFIGURATION OF THE EXPERIMENTAL SYSTEMS.

Method	Spreading gain	Digital up-carrier Carrier frequency	f_s	Analog up-carrier Carrier frequency
CSF-SM-DCSK	M= 40, P = 10	5 MHz	40 MHz	5 GHz
DCSK	640	-	40 MHz	5 GHz
NR-DCSK	640 (P = 10)	-	40 MHz	5 GHz
SOHS-DCSK	M= 40	5 MHz	40 MHz	5 GHz

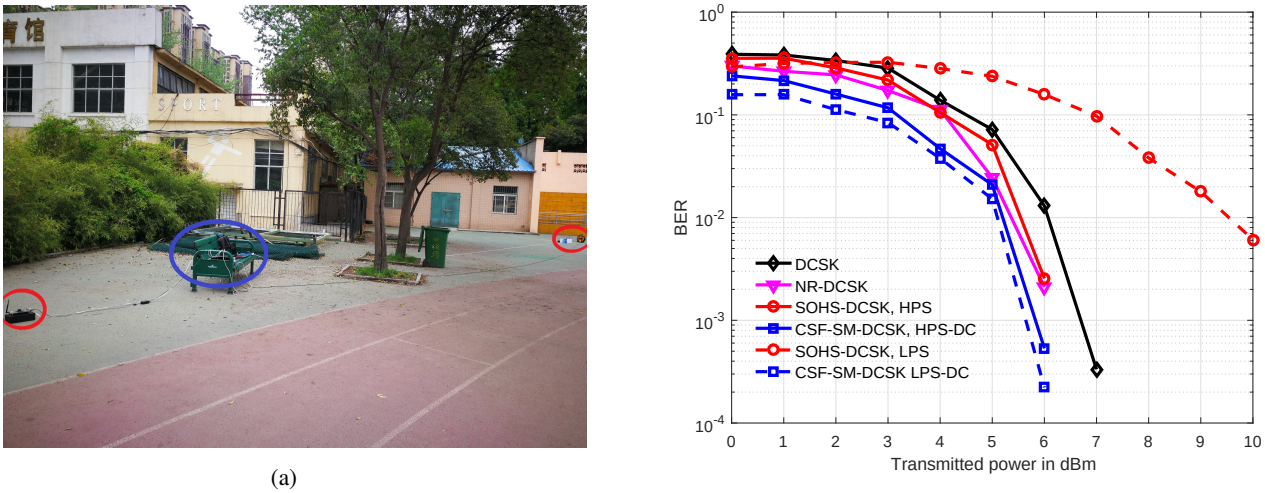

(a) (b)

Fig. 15. Field test of the different DCSK modulation schemes. (a) Picture of the test scenario and (b) Measured BER performance of the implemented radio links.

not only prove and validate the feasibility of the new CSF-SM-DCSK modulation scheme, but also show its superiority over its competitors known from the literature.

VI. Conclusions

A new CSF-SM-DCSK modulation scheme, which can transmit two data streams simultaneously, is proposed in this work. The high-priority channel relies on DCSK modulation, while the low-priority channel implements a coherent chaos-based spread spectrum communication system. The data streams transmitted via these channels are referred to as HPS and LPS, respectively. The CSF-SM-DCSK modulation combines many communications technologies to achieve superior noise and multipath performances. The chaotic carrier is generated by a chaotic shape-forming filter instead of a chaotic signal generator. Therefore, a coherent matched filter can be used at the receiver to demodulate the LPS data stream. Each LPS bit is encoded into a spreading code which improves both the noise and multipath performance of the LPS channel. The HPS channel uses the modulated LPS signal as a carrier and applies the DCSK modulation technique to the modulated LPS signal. The reference and information-bearing parts of DCSK signal are transmitted by two orthogonal sinusoidal carriers in the same time slot. Because of the simultaneous transmission, the HPS data rate is doubled, and both the transmitted and the receiver can be built without analog delay lines. Because of the DCSK modulation, the modulated LPS signal is transmitted twice, once as the reference and once as the information-bearing part of DCSK signals. The receiver of the proposed system includes a demodulator and a data corrector blocks to exploit all possible redundancy in the received signal. Using a correlator, the demodulator estimates the HPS bit, then removes the DCSK

modulation, and finally generates three data streams from the received signal. Two of them carry only the LPS data streams while the third one carries both the LPS and DCSK modulations. These data streams are processed by the data corrector, which provides enhanced versions of the LPS and HPS data streams.

Closed-form equations have been derived to predict the BER performances in both the HPS and LPS channels. Computer simulations have shown that the system performance of CSF-SM-DCSK modulation are in a very good agreement with the predicted one. The computer simulator has also been used to compare the system performance of CSF-SM-DCSK with its peers in AWGN and multipath radio channels. The results of simulations have shown that CSF-SM-DCSK substantially outperforms the system performance of its competitors known from literature, including conventional DCSK, NR-DCSK and SOHS-DCSK modulations in both the LPS and HPS channels. Besides that, the two independent data communications channels increase the channel capacity.

The new modulation scheme can be implemented on hardware platforms developed for the conventional communications systems. A CSF-SM-DCSK radio link has been implemented on a wireless open-access research platform, and its feasibility and performance have been proven and evaluated in a real application scenario. The WARP testbed has also been used to compare the system performances of different DCSK systems in real field tests. The results of real measurements have shown the superiority of the new CSF-SM-DCSK modulation scheme.

ACKNOWLEDGMENT

This research has been supported in part by the Scientific and Technological Innovation Leading Talents Program of Shaanxi Province, China Postdoctoral Science Foundation Funded Project (2020M673349) and Open Research Fund from Shaanxi Key Laboratory of Complex System Control and Intelligent Information Processing (2020CP02). (Corresponding author: Hai-Peng Ren, e-mail: renhaipeng@xaut.edu.cn)

REFERENCES

[1] L. M. Pecora, and T. L. Carroll, “Synchronization in chaotic systems,” *Phys. Rev. Lett.*, vol. 64, no. 8, pp. 821-824, Feb. 1990.

[2] S. Hayes, C. Grebogi, and E. Ott, “Communicating with chaos,” *Phys. Rev. Lett.*, vol. 70, no. 20, pp. 3031-3034, Jun. 1993.

[3] T. L. Carroll, “Communication with unstable basis functions,” *Chaos Soltion. Fract.*, vol. 104, pp. 766-771, Nov. 2017.

[4] J. Zhan, L. Wang, M. Katz, and G. R. Chen, “A differential chaotic bit-interleaved coded modulation system over multipath Rayleigh channels,” *IEEE Trans. Comm.*, vol. 65, no. 12, pp. 5257-5265, Dec. 2017.

[5] M. Dawa, G. Kaddoum, and Z. Sattar, “A generalized lower bound on the bit error rate of DCSK systems over multi-path Rayleigh fading channels,” *IEEE Trans. Circuits Syst. II, Exp. Briefs*, vol. 65, no. 3, pp. 321-325, Mar. 2018.

[6] J. M. Kim, B. V. Nguyen, H. Jung, and K. Kim, “TH-NRDCSK: A non-coherent time hopping chaotic system for anti-jamming communications,” *IEEE Access*, vol. 7, pp. 144710-144719, Sep. 2019.

[7] G. Kaddoum. "Wireless chaos-based communication systems: a comprehensive survey," *IEEE Access*, vol. 4, pp. 2621-2648, May 2016.

[8] A. Apostolos, S. Dimitris, L. Larger, et al. "Chaos-based communications at high bit rates using commercial fiber-optic links," *Nature*, vol. 438, no. 7066, pp.343-346, Nov. 2005.

[9] "IEEE Std 802.15.6-2012." *IEEE standard for local and metropolitan area networks-Part 15.6: Wireless body area networks,* 2012.

[10] G. Kolumbán, B. Vizvari, W. Schwarz, and A. Abel, "Differential chaos shift keying: A robust coding for chaotic communication," *in Proc. Int. Workshop Nonlinear Dyn. Electron. Syst.*, pp. 87-92, Jan. 1996.

[11] Y. Fang, G. J. Han, P. P. Chen, "A survey on DCSK-based communication systems and their application to UWB scenarios," *IEEE Commun. Surv. Tut.*, vol. 18, no. 3, pp. 1804-1837, May 2016.

[12] G. Kaddoum, and E. Soujeri, "NR-DCSK: A noise reduction differential chaos shift keying system," *IEEE Trans. Circuits Syst. II, Exp. Briefs*, vol. 63, no. 7, pp. 648-652, Jul. 2016.

[13] W. K. Xu, L. Wang, and G. Kolumbán, "A novel differential chaos shift keying modulation scheme," *Int. J. Bifurc. Chaos*, vol. 21, no. 3, pp. 799-814, Mar. 2011.

[14] F. C. M. Lau, and C. K. Tse, "Chaos-based digital communication systems," *Heidelberg, Germany: Springer-Verlag*, 2003.

[15] G. Kaddoum, E. Soujeri, C. Arcila, and K. Eshteiwi, "I-DCSK: An improved noncoherent communication system architecture," *IEEE Trans. Circuits Syst. II, Exp. Briefs*, vol. 62, no. 9, pp. 901-905, May 2015.

[16] C. Bai, H. P. Ren, and C. Grebogi, "Experimental phase separation differential chaos shift keying wireless communication based on matched filter," *IEEE Access*, vol. 7, no. 1, pp. 25274-25287, Feb. 2019.

[17] H. Yang, G. P. Jiang, and J. Y. Duan, "Phase-Separated DCSK: A simple delay-component-free solution for chaotic communications," *IEEE Trans. Circuits Syst. II, Exp. Briefs*, vol. 61, no. 12, pp. 967-971, Sep. 2014.

[18] F. Taleb, D. Roviras, and F. T. Bendimerad, "Very high efficiency differential chaos shift keying system with Walsh hadamard codes," *Proceeding of IEEE Multimedia Computing and Systems(ICMCS)*, pp. 523-527, Apr. 2016.

[19] G. Kaddoum, and F. Gagnon, "Design of a high-data-rate differential chaos-shift keying system," *IEEE Trans. Circuits Syst. II, Exp. Briefs*, vol.59, no.7, pp.448-452, Jun. 2012.

[20] G. Kolumbán, Z. Jákó, and M. P. Kennedy, "Enhanced versions of DCSK and FM-DCSK data transmission systems," *in Proc. IEEE-ISCAS*, vol. 4, pp. 475-478, May/Jun. 1999.

[21] G. Kaddoum, F. Gagnon, and F. D. Richardson, "Design and analysis of a multi-carrier differential chaos shift keying communication system," *IEEE Trans. Commun.*, vol. 61, no. 8, pp. 3281-3291, Aug. 2013.

[22] G. X. Cheng, L. Wang, W. K. Xu, and G. R. Chen, "Carrier index differential chaos shift keying modulation," *IEEE Trans. Circuits Syst. II, Exp. Briefs*, vol. 64, no. 8, pp. 907-911, Oct. 2017.

[23] H. Yang, G. P. Jiang, W. K. S. Tang, G. R. Chen, and Y. C. Lai, "Multi-carrier differential shift keying system with subcarriers allocation for noise reduction," *IEEE Trans. Circuits Syst. II, Exp. Briefs*, vol. 65, no. 11, pp. 1733-1737, Sep. 2018.

[24] X. Q. Nguyen, "Multi-carrier differential shift keying system with repeated spreading sequence," *J. Commun. Netw.*, vol. 20, no. 3, pp. 299-308, Mar. 2018.

[25] G. F. Cai, Y. Fang, G. J. Han, F. C. M. Lau, and L. Wang, "A square-constellation-based M-ary DCSK communication system," *IEEE Access*, vol. 4, pp. 6295-6303, Sep. 2016.

[26] T. T. Huang, L. Wang, W. K. Xu, and F. C. M. Lau, "Multilevel code-shifted differential-chaos-shift-keying system," *IET communications*, vol. 10, no. 10, pp. 1189-1195, Jul. 2016.

[27] H. P. Ren, M. S. Baptista, and C. Grebogi, "Wireless communication with chaos," *Phy. Rev. Lett.*, 110, 18, pp. 184101, May 2013.

[28] H. P. Ren, C. Bai, and C. Grebogi, "Chaotic shape-forming filter and corresponding matched filter in wireless communication," *Advances on Nonlinear Dynamics of Electronic Systems, Singapore: World Scientific Press*, 2019.

[29] N. J. Corron, and J. N. Blakely, "Chaos in optimal communication waveforms," *Proc. R. Soc. A*, vol. 471, no. 2180, pp. 20150222, Aug. 2015.

[30] J. L. Yao, Y. Z. Sun, H. P. Ren, and C. Grebogi, "Experimental wireless communication using chaotic baseband waveforms," *IEEE Trans. Vhe. Technol.*, vol. 68, no. 1, pp. 578-591, Jan. 2019.

[31] J. L. Yao, C. Li, H. P. Ren, and C. Grebogi, "Chaos-based wireless communication resisting multipath effects," *Phy. Rev. E*, vol. 96, pp. 032226, Sep. 2017.

[32] C. Bai, H. P. Ren, W. Y. Zheng, and C. Grebogi, "Radio-wave communication with chaos," *IEEE Access*, vol. 8, pp. 167019-167026, Sep. 2020.

[33] H. P. Ren, H. P. Yin, H. E. Zhao, C. Bai, and C. Grebogi, "Artificial Intelligence Enhances the Performance of Chaotic Baseband Wireless Communication," *IET Commun.*, online 2021/03/26 DOI: 10.1049/cmu2.12162.

[34] H. P. Yin, and H. P. Ren, "Direct Symbol Decoding using GA-SVM in Chaotic Baseband Wireless Communication System," *J. Franklin Institute*, online 2021/06/21 DOI: 10.1016/j.jfranklin.2021.06.012.

[35] H. P. Ren, H. P. Yin, C. Bai, and J. L. Yao, "Performance improvement of chaotic baseband wireless communication using echo state network," *IEEE Trans. Commun.*, vol. 68, no. 10, pp. 6525-6536, Jul. 2020.

[36] C. Bai, H. P. Ren, and G. Kolumbán, "Double-sub-stream M-ary differential chaos shift keying wireless communication system using chaotic shape-forming filter," *IEEE Trans. Circuits Syst. I, Reg. Papers,* vol. 67, no. 10, pp. 3574-3587, Oct. 2020.

[37] Y. Wang, L. Zhang, and Z. Q. Wu, "Robust MUI suppression for MIMO visible light communication system with location-aided chaotically rotating orthogonal scheme," *IEEE Comm. Lett.*, vol. 23, no. 8, pp. 1361-1364, Jun. 2019.

[38] X. M. Cai, W. K. Xu, and D. Q. Wang, "An M-ary orthogonal multilevel differential chaos shift keying system with code index modulation," *IEEE Trans. Commun.*, vol. 67, no. 7, pp. 4835-4847, Mar. 2019.

[39] E. Rosa, S. Hayes, and C. Grebogi, "Noise filtering in communication with chaos," *Phys. Rev. Lett.*, vol. 78, no. 7, pp. 1247-1250, Feb. 1997.

[40] C. Li, G. Luo, and K. Qin, "An image encryption scheme based on chaotic tent map," *Nonlinear Dyn.*, vol. 87, no. 1, pp. 127-131, Aug. 2017.

[41] F. J. Escribano, L. Lopez, and M. A. F. Sanjuan, "Chaos-coded modulations over Rician and Rayleigh flat fading channels," *IEEE Trans. Circuits and Syst. II, Exp. Briefs*, vol. 55, no. 6, pp. 581-585, Jun. 2008.

[42] T. Cover, "Broadcast channels," *IEEE Trans. Inf. Theory*, vol. IT-18, no. 1, pp. 2-14, Jan. 1972.

[43] J. Hong, and P. Wilford, "A hierarchical modulation for upgrading digital broadcast systems," *IEEE Trans. Broadcast*, vol. 51, no. 2, pp. 223-229, Jun. 2005.

[44] S. Wang, S. Kwon, and B. K. Yi, "On enhancing hierarchical modulation," *IEEE Int. Symposium on Broadband Multimedia Systems and Broadcasting*, Apr. 2008, pp. 1-6.

[45] L. Wang, G. F. Cai, and G. R. Chen, "Design and performance analysis of a new multi-solution M-ary differential chaos shift keying communication system," *IEEE Trans. Wireless Commun.*, vol. 14, no. 9, pp. 5194-5208, Sep. 2015.

[46] G. F. Cai, Y. Fang, G. J. Han, L. Wang, and G. R. Chen, "A new hierarchical M-ary DCSK communication system: design and analysis," *IEEE Access*, vol. 5, pp. 17414-17424, Aug. 2017.

[47] G. F. Cai, Y. Fang, and G. J. Han, "Design of an adaptive multi-resolution M-ary DCSK system," *IEEE Comm. Lett.*, vol. 21, no. 1, Sep. 2017.

[48] H. P. Ren, C. Bai, J. Liu, M. S. Baptista, and C. Grebogi, "Experimental validation of wireless communication with chaos," *Chaos*, vol. 26, no. 8, 083117, Aug. 2016.

[49] N. J. Corron, J. N. Blakely, and M. T. Stahl, "A matched filter for chaos," *Chaos*, vol. 20, no. 2, pp. 023123, Jun. 2010.

[50] T. S. Rappaport, *Wireless communications: Principle and practice*. Prentice-Hall, 1996.

[51] G. Kaddoum, F. D. Richardson, and F. Gagnon, "Design and analysis of a multi-carrier differential chaos shift keying communication system," *IEEE Trans. Commun.*, vol. 61, no. 8, pp. 3281-3291, Aug. 2013.

[52] N. X. Quyen, "Multi-carrier differential chaos-shift keying with repeated spreading sequence," *J. Commun. Net.*, vol. 20, no. 3, pp. 299-308, Jun. 2018.

[53] N. X. Quyen, "Quadrature MC-DCSK scheme for chaos-based cognitive radio," *Int. J. Bifurcat. Chaos*, vol. 29, no. 13, pp. 1950177, Mar. 2019.

[54] J. N. Blakely, D. W. Hahs, and N. J. Corron, "Communication waveform properties of an exact folded-band chaotic oscillator," *Phys. D*, vol. 263, no. 22, pp. 99-106, Nov. 2013.

[55] N. J. Corron, J. N. Blakely, and M. T. Stahl, "Erratum: A matched filter for chaos," *Chaos*, vol. 22, pp. 023123, May 2012.

[56] *Wireless Open Access Research Platform.* Accessed: 2020. [Online]. Available: http://warp.rice.edu

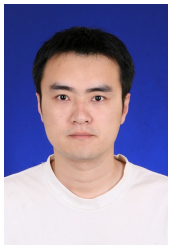

Chao Bai was born in Xi'an, China, in 1988. He received the B. S. degree in Automation from Xi'an Polytechnic University in 2010, and received the M. S. degree and P.h.D degree in control science and engineering from Xi'an University of Technology in 2014 and 2019, respectively. He holds a post-doctoral position with Xi'an Technological University. He has published more than ten journal articles and held five patents. His current research interests are chaotic communication and complex networks.

Xiao-Hui Zhao was born in Xian, China, in 1995. He received the B. S. degree in Automation from Shaanxi University of Technology, and the M. S. degree in control engineering from Xi'an University of Technology, in 2017 and 2021, respectively. His research interests include chaotic communication and data encryption.

Hai-Peng Ren was born in Heilongjiang, China, March 1975. He got doctor degree on power electronics and power drives from Xi'an university of Technology in 2003. He worked as a visiting researcher in the field of nonlinear phenomenon of power converters in Kyushu University, Japan, from April 2004 to October 2004. He worked as post PH.D. research fellow in the field of time-delay system in Xi'an Jiaotong University from December 2005 to December 2008. He worked as an honorary visiting professor in the field of communication with chaos and complex networks in University of Aberdeen, Scotland, from July 2010 to July 2011. From December 2008 to June 2018, he worked as a professor at the department of information and control engineering, Xi'an University of Technology, Xi'an, China. From July 2018, he moved to Xian Technological University. His field includes nonlinear system control, complex networks and communication with nonlinear dynamics.

Géza Kolumbán Fellow of IEEE (2005), IEEE CAS Distinguished Lecturer (2013-2014), was graduated from and received his Ph.D. at the Technical University of Budapest and received his C.Sc. and D.Sc. degrees from the Hungarian Academy of Sciences. He spent 15 years in the telecommunications industry where he developed microwave circuits, PLL-based frequency synthesizers and was involved in many system engineering projects from satellite telecommunications to microwave digital radio systems. After joining the university education he showed that chaos may exist in autonomous PLLs and established noncoherent chaotic communications as a brand new research direction. He developed DCSK and FM-DCSK, the most popular chaotic modulation schemes. Two of his papers, written on chaos-based communications, have been ranked in the top cited IEEE Trans. CAS-I articles. He elaborated a unified theory for the Software Defined Electronics (SDE) systems and received the ICT Expresss Best Paper Award in 2017 for the SDE concept. He has been a visiting professor and researcher to UC Berkeley, PolyU and CityU in Hong Kong, University College Dublin and Cork, Ireland, EPFL, Lausanne, Switzerland, INSA-LATTIS Laboratory, Toulouse, France, TU Dresden, Germany, Beijing Jiaotong University, China. Prof. Kolumbán has been providing consulting service for many companies from Samsung Advanced Institute of Technology to National Instruments. He is a full professor at the Pázmány Péter Catholic University, Budapest, Hungary and is an Adjunct Prof. at the Edith Cowan University, Perth, Australia. He served/is serving as an Associate Editor at IEEE TCAS-II, ICT Express, Elsevier DSP and Dynamics of Continuous, Discrete and Impulsive Systems, Series B.

Celso Grebogi got his PhD in Physics from the University of Maryland in 1978, Postdoc in Physics and Applied Mathematics at UC Berkeley in 1978-1981. He is the Sixth Century Chair, and the Founding Director of the Institute for Complex Systems and Mathematical Biology, Kings College, University of Aberdeen, UK. He is also an External Scientific Member (Mitglied) of the Max-Planck-Society. He was previously with the University of Sao Paulo as Full Professor of Physics, and, before that, with the University of Maryland as Full Professor of Mathematics. He has made a major impact for his work in the field of chaotic and complex dynamics. He was awarded the Senior Humboldt Prize and the Thomson-Reuters Citation Laureate. The seminal work on chaos control (OGY) was selected by the American Physical Society as a milestone in the last 50 years. He received multiple Doctor Honoris Causa degrees, Humboldt Senior Prize, Fulbright Fellowship, Toshiba Chair, and various Honorary Professorship awards. He is Fellow of the Royal Society of Edinburgh, The World Academy of Sciences, Academia Europaea, Brazilian Academy of Sciences, American Physical Society, and the UK Institute of Physics.